Scientia Iranica (2025) **32**(2): 6746

SCIENTIA IRANICA

Sharif University of Technology
Scientia Iranica
Transactions on Mechanical Engineering
https://scientiairanica.sharif.edu

Four-variable quasi-3D model for nonlinear thermal vibration of FG plates lying on Winkler-Pasternak-Kerr foundation

Belgacem Mamen [a,b], Abdelhakim Bouhadra [a,b], Fouad Bourada [a,c], Mohamed Bourada [a], Abdelouahed Tounsi [a,d,e,f,*], Muzamal Hussain [g]

a. Department of Civil Engineering Material and Hydrology Laboratory, Faculty of Technology, University of Sidi Bel Abbes, Khenchela, Algeria.
b. Department of Civil Engineering, Faculty of Science &Technology, Abbes Laghrour University, Khenchela, Algeria.
c. Départment des Sciences et de la Technologie, Université de Tissemsilt, Hamouda, Algérie.
d. Yonsei Frontier Lab, Yonsei University, Seoul, Korea.
e. Department of Civil and Environmental Engineering, King Fahd University of Petroleum & Minerals, Dhahran, Eastern Province, Saudi Arabia.
f. Interdisciplinary Research Center for Construction and Building Materials, KFUPM, Dhahran, Saudi Arabia.
g. Department of Mathematics, Govt. College University Faisalabad, Faisalabad, Pakistan.

* Corresponding author: tou_abdel@yahoo.com (A. Tounsi)

Received 28 April 2022; received in revised form 31 January 2023; accepted 10 March 2024

Keywords

Nonlinear thermodynamic;
FG plates;
Winkler/Pasternak/Kerr foundation;
Temperature-dependence material.

Abstract

This paper presents the nonlinear thermodynamic results of Functionally Graded (FG) plates lying on Winkler/Pasternak and Kerr foundation through an analytical formulation. The field displacement is defined by only four unknowns, including an indeterminate integral and a new shape function representing the transverse shear stresses. Material properties of the FG plates are temperature-dependent and graded according to a simple power-law distribution. Also, the thermodynamic equations of motion are deduced based on Hamilton's principle. The exactitude of the present theory results is verified with those obtained by various researchers. The effects of temperature-dependence material properties, power-law index, nonlinear temperature rising, elastic foundation parameters, aspect, and slenderness ratio are discussed. The results show that the increase in elastic foundation parameters would enhance the thermodynamic response of the FG plates. Nevertheless, the degree of improvement would be related to the nonlinear temperature change. Moreover, the plate's configuration effect is more significant when the nonlinear temperature difference is high.

1. Introduction

The continuous evolution of thermomechanical properties between the lower and upper surfaces of Functionally Graded (FG) structures makes them widely used in diverse areas such as aerospace, nuclear reactors, power sources, biomechanical, optical, civil, automotive, electronic, chemical, and mechanical engineering [1].

The material features gradually differ along with one or various dimensions of the structure to achieve intended functionalities. Researchers developed FG materials to resist ultra-high temperatures. The FG structures have been tested under high-temperature gradients across the cross-sectional thickness [2]. This type of material is prepared by mixing two different constituents, such as ceramic and metal. This advanced manufacturing process aims at developing ideal heat-resistant materials. In this way, thermal resistance is provided by a heat-resistant ceramic on one side. At the same time, crack resistance is offered by metal with high thermal conductivity and high hardness. Thanks to these simultaneous functions, the use of Functionally Graded Materials (FGMs) has been fostered in thermal protection systems for melting reactors and heat exchanger pipes [3-9].

After their innovation in the late 90s, researchers carried out various investigations to assess the thermomechanical and dynamic behaviors of FGMs plates using different analytical methods [10-14]. Thai et al. [2] confirmed that the First Shear Deformation Theory (FSDT) is also accurate in investigating the free vibration analysis of FGM plates composed of FG face sheets and an isotropic homogeneous core with variable thickness. Ye et al. [15] recently analyzed

To cite this article:
B. Mamen, A. Bouhadra, F. Bourada, M. Bourada, A. Tounsi, M. Hussain "Four-variable quasi-3D model for nonlinear thermal vibration of FG plates lying on Winkler-Pasternak-Kerr foundation", *Scientia Iranica* (2025), **32**(2): 6746. https://doi.org/10.24200/sci.2024.60340.6746

2345-3605 © 2025 Sharif University of Technology. This is an open access article under the CC BY-NC-ND license.

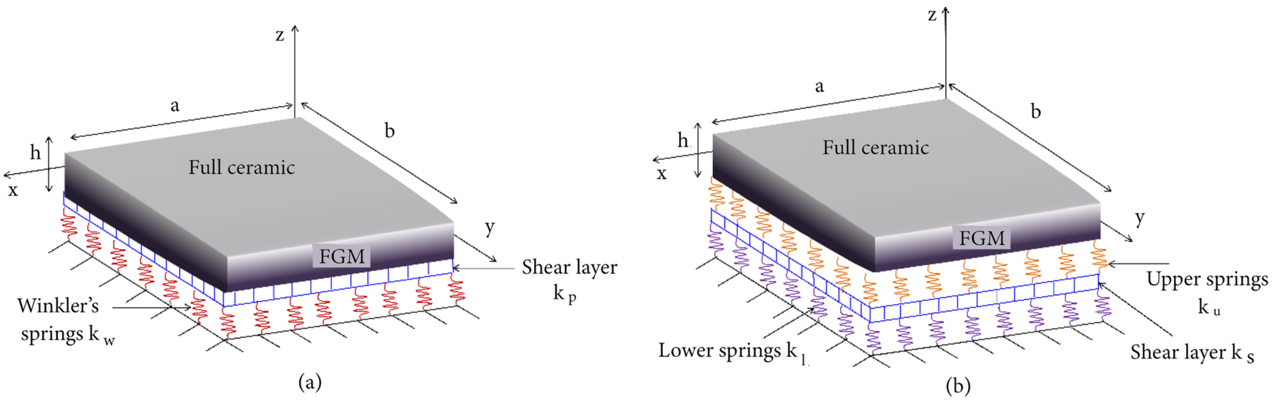

Figure 1. Geometry and coordinate system of FG square plates lying on elastic foundations (a) Winkler-Pasternak foundation, and (b) Kerr foundation.

the free vibration behavior of FG sandwich plates using new higher-order refined models.

As stated previously, to withstand the high temperatures, FGM structures made up of ceramic/metallic components are generally of interest. Shariyat [16] introduced a generalized global-local theory to investigate the vibration behavior of FG sandwich plates exposed to thermo-mechanical loads. Malekzadeh and Monajjemzadeh [17] investigated the thermal dynamic response of FG plates resting on elastic foundation and subjected to a moving load based on the first-order shear deformation theory, including the initial thermal stresses' effects. Two dimensions' free vibration responses of temperature-dependent FG plates have been analyzed by Attia et al. [18] using four-variable Higher-order Shear Deformation Theory (HSDT). Parida and Mohanty [6] employed HSDT to consider the free vibration response of rotating FG plates subjected to the nonlinear temperature. Zaoui et al. [19] studied the free vibration of FG temperature-dependent properties plates using an improved exponential-trigonometric two-dimensional higher shear deformation theory. Furthermore, Arshid et al. [20] analyzed the thermomechanical buckling and vibrational behavior of a sandwich-curved microbeam resting on the Visco-Pasternak foundation. Navier's solution method is used to solve the differential equations system analytically. Based on the findings, such intelligent structures can be used to design and manufacture various equipment, making high stiffness-to-weight ratios more accessible. Li et al. [21] investigated the nonlinear vibration behavior of FG sandwich beams. In thermal environments, the beams have been modeled with an auxetic porous copper core. Singha et al. [22] analyzed the vibration analysis of a rotating pre-twisted Graphene-Reinforced Composite (GRC) cylindrical shell. The temperature-dependent material properties of the FG-GRC have been predicted by employing the continued Halpin-Tsai model. Abouelregal et al. [23] analyzed the vibrational behavior of rotating isotropic nanobeams using the nonlocal theory of elasticity. This study aims to contribute to understanding the dynamics of rotating nanobeams subject to varying heat sources. Also, the thermoelastic vibrations of nanobeams resting on a Pasternak foundation and thermally loaded by ramp-type varying heat have been investigated by Nasr et al. [24].

Nevertheless, limited research has been carried out to analyze the 3D thermodynamic behavior of FG structures or those lying on Winkler, Pasternak, and Kerr foundation [25-27]. Malekzadeh et al. [25] investigated the three-dimensional thermal dynamic response of thick FG annular plates in a thermal environment. The Differential Quadrature Method (DQM) has been used to drive the 3D thermoelastic equilibrium equations. Tu et al. [27] have considered the heat conduction and temperature-dependent material properties to analyze FG plates' 3D free vibration behavior in thermal environments using an eight-unknown HSDT. On the one hand, Parida and Mohanty [6] and Zaoui et al. [28] are the only researchers investigating the nonlinear thermal vibration behavior of FG plates based on a displacement field containing four variables (2D-shear deformation theory). On the other hand, the main advantage of our study is to use a displacement field containing the same number of unknowns (four variables) with 3D theory. Additionally, this model simplifies the problem and considers the effect of transverse stretching, which is not considered in the case of 2D-shear deformation theories.

According to this literature, in all the previously mentioned research, the thermal conductivity has always been considered independent of temperature, affecting the obtained results when the temperature difference is at high levels. Therefore, this work deals with proposing a new 3D modelling concept and investigating the nonlinear temperature field effect on the free vibration behavior of FG plates resting on various elastic foundations. Even more, the implications of temperature-dependent material properties, power-law property index, non-linear temperature rise, elastic foundation parameters, and aspect ratio and slenderness ratio are reviewed.

2. FG plates

The considered plates of length *(a)*, width *(b)*, and thickness *(h)* lie on elastic foundations (Winkler-Pasternak foundation and Kerr foundation). All the investigated plates are exposed to the nonlinear temperature change, see Figure 1. Mechanical characteristics vary progressively with thickness, from the lower metal surface to the upper ceramic surface.

Significantly, to more accurately describe the behavior of FG plates at elevated temperatures, the material parameters need to be temperature-dependent $P(z,T)$, including Poisson's ratio, Young's modulus, the thermal expansion, and the thermal conductivity are presented as [29,30]:

$$P(z,T) = [P_c(T) - P_m(T)]V_c + P_m(T), \tag{1}$$

where $P_m(T)$ and $P_c(T)$ denote the effective temperature-dependent properties of the metal and ceramic, respectively. V_c denotes the ceramic fraction and it is given conforming to the power law:

$$V_c = \left(\frac{1}{2} + \frac{z}{h}\right)^k, \tag{2}$$

in which k is the volume fraction exponent.

Touloukian [31] suggests the material properties as follows:

$$P(T)_i = P_0(P_{-1}T^{-1} + 1 + P_1T + P_2T^2 + P_3T^3), \tag{3}$$

where i = c, m. T is temperature in Kelvin, and P_j (j = −1,1,0,1,2,3) are the temperature-dependent factors, see Table 1, Mamen et al. [30]. Also, the variation of the effective temperature-dependent and independent material properties is illustrated in Figure 2.

Figure 2(a)–(c) show the evolution of temperature-dependent properties through the FG square plate's thickness. The temperature of the lower surface is constant (T_m = 300 K), while the upper surface temperature is varied (T_c =300 to 700 K). It can find that the temperature has an important influence on all material properties except Poisson's coefficient. Therefore, in this investigation, Poisson's coefficient will be considered a constant (independent of temperature) and equals 0.28.

Table 1. Factor defining the temperature dependence of Si_3N_4 and SUS304 [30, 40].

Constituents	Properties	P_0	P_{-1}	P_1	P_2	P_3
SUS304	E (Pa)	201.04e+9	0	3.079e−4	−6.534e−7	0
	α (K^{-1})	12.330−6	0	8.086e−4	0	0
	κ (Wm^{-1}K^{-1})	15.379	0	−1.264e−3	2.092e−6	−7.223e−10
	ν	0.3262	0	−2.002e−4	3.797e−7	0
	ρ (kg/m^3)	8166	0	0	0	0
Si_3N_4	E (Pa)	348.43e+9	0	−3.070e−4	2.160e−7	−8.946e−11
	α (K^{-1})	5.8723e−6	0	9.095−4	0	0
	κ (Wm^{-1}K^{-1})	13.723	0	−1.032−3	5.466e−7	−7.876e−11
	ν	0.24	0	0	0	0
	ρ (kg/m^3)	2370	0	0	0	0

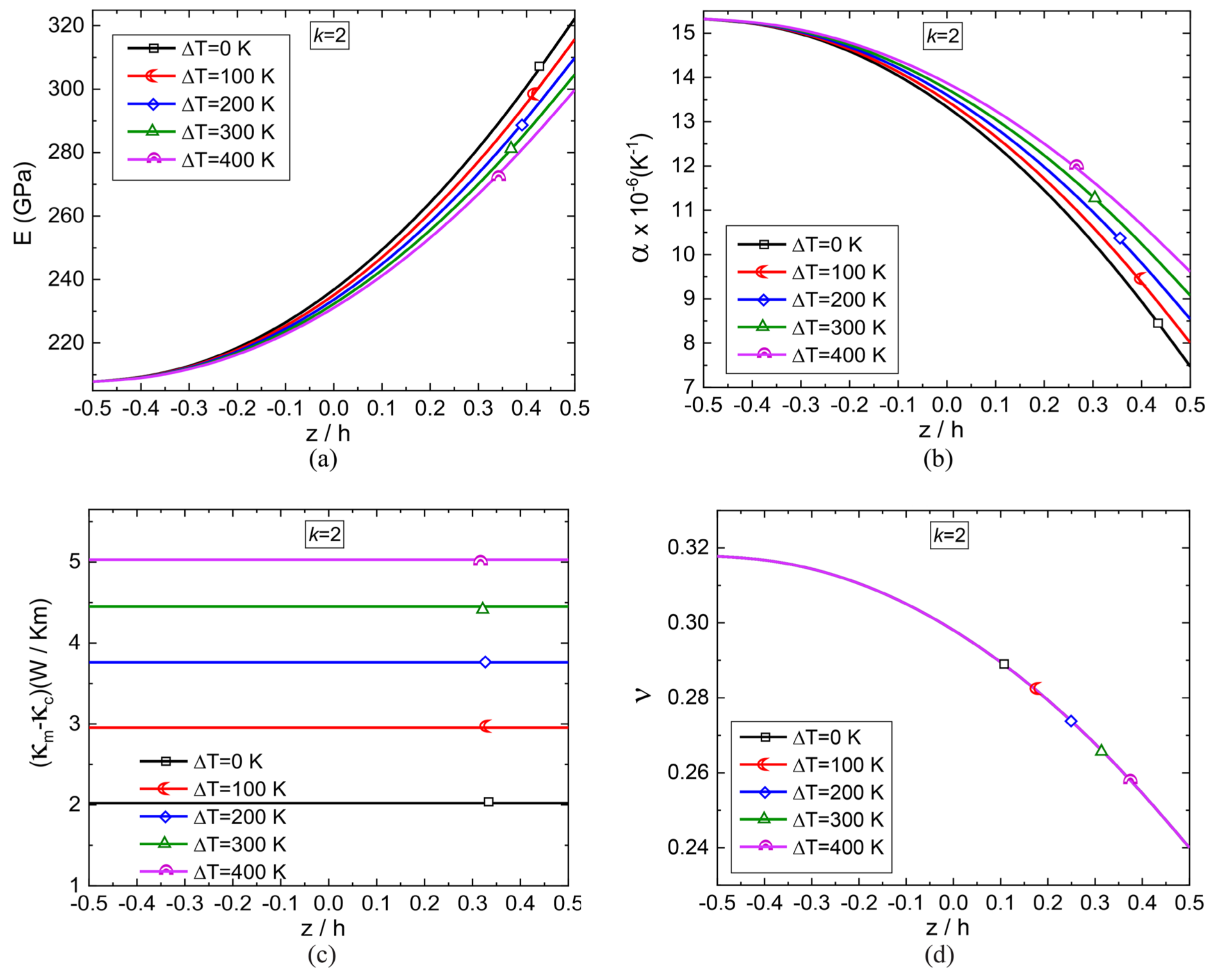

Figure 2. Temperature-dependent properties through the FG square plates' thickness (a) Young's modulus, (b) thermal expansion coefficient, (c) thermal conductivity, and (d) Poisson's coefficient.

3. Nonlinear temperature distribution

Assume the FGM plates are exposed to Non-Linear Temperature Rise (NLTR). The temperature field distributes nonlinearly from the upper surface T_c to the lower surface T_m=300 K. In this case, the one-dimensional steady-state heat conduction along the thickness is given as Salari et al. [32]:

$$-\frac{d}{dz}\left[\kappa(z,T)\frac{dT(z)}{dz}\right]=0. \quad (4)$$

Taking into account the continuous thermal conditions yield to:

$$T(z)=T_m+\Delta T\frac{\int_{-h/2}^{z}\frac{1}{\kappa(z,T)}dz}{\int_{-h/2}^{h/2}\frac{1}{\kappa(z,T)}dz},-\frac{h}{2}\le z\le\frac{h}{2}, \quad (5)$$

in which $\Delta T=T_c-T_m$.

Eq. (5) can be solved by using an approximation of polynomial series expansion [30, 33-35]:

$$T(z)=T_m+(T_c-T_m)\frac{D_1(z)}{D_0(z)}, \qquad -\frac{h}{2}\le z\le\frac{h}{2}, \quad (6)$$

$$D_j(z)=\sum_{i=0}^{r}\left(\frac{\kappa_m-\kappa_c}{\kappa_m}\right)^i\frac{\left(\frac{1}{2}+\frac{z}{h}\right)^{(in+1)j}}{in+1}, \quad j=0,1. \quad (7)$$

where r represents the item numbers in the series and is chosen equals to five to ensure the computation is accurate.

4. Theory and governing equations

4.1. Kinematics and constitutive relations

The boundary conditions are the main limitation of the present model compared to computational methods. In other words, the present model could be only used for simply-supported plates. However, with a slight modification in solutions (functions in the double Fourier series), the present model could effectively predict the behavior of clamped or simply-clamped FG plates.

Based on 2D and 3D higher shear deformation theories, the fields of displacement are described as follows:

$$\begin{aligned}
u(x,y,z,t)&=u_0(x,y,t)-z\frac{\partial w_0(x,y,t)}{\partial x}+K_1f(z)\int\theta(x,y,t)dx,\\
v(x,y,z,t)&=v_0(x,y,t)-z\frac{\partial w_0(x,y,t)}{\partial y}+K_2f(z)\int\theta(x,y,t)dy,\\
w(x,z,t)&=w_0(x,y,t)+ng(z)\theta(x,y,t).
\end{aligned} \quad (8)$$

The undetermined integral in Eq. (8) is simplified and declared as [36]:

$$\int\theta(x,y,t)\,dx=A'\frac{\partial\theta(x,y,t)}{\partial x}, \quad (9)$$

$$\int\theta(x,y,t)\,dy=B'\frac{\partial\theta(x,y,t)}{\partial y}. \quad (10)$$

Based on Eqs. (9) and (10), Eq. (8) takes the following form:

$$\begin{cases}
u(x,y,z,t)=u_0(x,y,t)-z\frac{\partial w_0(x,y,t)}{\partial x}+k_1A'f(z)\frac{\partial\theta(x,y,t)}{\partial x},\\
v(x,y,z,t)=v_0(x,y,t)-z\frac{\partial w_0(x,y,t)}{\partial y}+k_2B'f(z)\frac{\partial\theta(x,y,t)}{\partial y},\\
w(x,y,z,t)=w_0(x,y,t)+ng(z)\theta(x,y,t),
\end{cases} \quad (11)$$

where u_0, v_0, w_0, and θ are unknown displacements of the mid-plane of the FGM plate. where the coefficients (k_1,k_2) and (A',B') are defined as:

$$k_1=-\lambda^2 \text{ and } A'=-\frac{1}{\lambda^2}, \quad (12)$$

$$k_2=-\beta^2 \text{ and } B'=-\frac{1}{\beta^2}. \quad (13)$$

Note that λ and β are defined in Eq. (62).

f(z) represents the shape function defining the distribution of transverse shear deformation, it is written as follows [30]:

$$f(z)=z\left(\frac{27}{4}-9z^2\right) \text{ and } g(z)=\frac{2}{15}\frac{df(z)}{dz}. \quad (14)$$

n is a real number and is given as follows:

$$\begin{cases} n=0 \text{ for 2D} \\ n=1 \text{ for Quasi-3D}\end{cases}. \quad (15)$$

The deformations associated with displacements in Eq. (11) are:

$$\varepsilon_x=\frac{\partial u_0}{\partial x}-z\frac{\partial^2 w_0}{\partial x^2}+k_1A'f(z)\frac{\partial^2\theta}{\partial x^2}, \quad (16)$$

$$\varepsilon_y=\frac{\partial v_0}{\partial y}-z\frac{\partial^2 w_0}{\partial y^2}+k_2B'f(z)\frac{\partial^2\theta}{\partial y^2}, \quad (17)$$

$$\varepsilon_z=g'(z)\theta, \quad (18)$$

$$\gamma_{xz}=\frac{\partial\theta}{\partial x}[k_1A'f'(z)+g(z)], \quad (19)$$

$$\gamma_{yz}=\frac{\partial\theta}{\partial y}[k_2B'f'(z)+g(z)], \quad (20)$$

$$\gamma_{xy}=\frac{\partial u_0}{\partial y}-2z\frac{\partial^2 w_0}{\partial x\partial y}+k_1f(z)A'\frac{\partial^2\theta}{\partial x\partial y}+\frac{\partial v_0}{\partial x}+k_2f(z)B'\frac{\partial^2\theta}{\partial x\partial y}, \quad (21)$$

where $\varepsilon_x, \varepsilon_y$, and ε_z are the normal and the transverse strains, and $\gamma_{xz}, \gamma_{yz}, \gamma_{xy}$ are the transverse shear strains.

Based on 3D displacement field expressed in Eq. (11), the linear constitutive relations are given as:

$$\begin{Bmatrix}\sigma_x\\ \sigma_y\\ \sigma_z\\ \tau_{yz}\\ \tau_{xz}\\ \tau_{xy}\end{Bmatrix}=\begin{bmatrix}C_{11}&C_{12}&C_{13}&0&0&0\\ C_{12}&C_{22}&C_{23}&0&0&0\\ C_{13}&C_{23}&C_{33}&0&0&0\\ 0&0&0&C_{44}&0&0\\ 0&0&0&0&C_{55}&0\\ 0&0&0&0&0&C_{66}\end{bmatrix}\begin{Bmatrix}\varepsilon_x\\ \varepsilon_y\\ \varepsilon_z\\ \gamma_{yz}\\ \gamma_{xz}\\ \gamma_{xy}\end{Bmatrix}. \quad (22)$$

The effective temperature-dependent elastic constants $C_{ij}(z,T)$ depending on the normal strain ε_z are given as follows:

Case of 2D ($\varepsilon_z = 0$), then C_{ij} are:

$$C_{11}=C_{22}=\frac{E(z,T)}{1-\nu(z,T)^2},$$
$$C_{12}=\frac{\nu(z,T)E(z,T)}{1-\nu(z,T)^2},$$
$$C_{44}=C_{55}=C_{66}=\frac{E(z,T)}{2[1+\nu(z,T)]}. \quad (23)$$

Case of quasi–3D ($\varepsilon_z \neq 0$), then C_{ij} are:

$$C_{11}=C_{22}=C_{33}=\frac{E(z,T)[1-\nu(z,T)]}{[1-2\nu(z,T)][1+\nu(z,T)]},$$
$$C_{12}=C_{13}=C_{23}=\frac{\nu(z,T)E(z,T)}{[1-2\nu(z,T)][1+\nu(z,T)]},$$
$$C_{44}=C_{55}=C_{66}=\frac{E(z,T)}{2[1+\nu(z,T)]}. \quad (24)$$

4.2. Governing equations of motion

By employing the Hamilton principle in its analytical form, the three governing equations are developed as follows [30, 37]:

$$\int_{t_1}^{t_2}\delta\big(U+P_f+V-K\big)\,dt=0, \quad (25)$$

in which t_1 and t_2 are the initial and end times, respectively.

The change of the total strain energy is represented as [38]:

$$\delta U=\int_V \sigma_{ij}\delta\varepsilon_{ij}\,dV, \quad (26)$$

$$\delta U=\int_{-\frac{h}{2}}^{+\frac{h}{2}}\int_0^a\int_0^b\begin{pmatrix}\sigma_x\delta\varepsilon_x+\sigma_y\delta\varepsilon_y+\sigma_z\delta\varepsilon_z\\ +\tau_{xz}\delta\gamma_{xz}+\tau_{yz}\delta\gamma_{yz}+\tau_{xy}\delta\gamma_{xy}\end{pmatrix}dzdx, \quad (27)$$

$$\delta U=\int_0^a\int_0^b\begin{bmatrix}N_x\frac{\partial\delta u_0}{\partial x}-M_x^b\frac{\partial^2\delta w_0}{\partial x^2}\\ +k_1A'M_x^s\frac{\partial^2\delta\theta}{\partial x^2}+N_y\frac{\partial\delta v_0}{\partial y}\\ -M_y^b\frac{\partial^2\delta w_0}{\partial y^2}+k_2B'M_y^s\frac{\partial^2\delta\theta}{\partial y^2}\\ +N_z\delta\theta+N_{xy}\frac{\partial\delta u_0}{\partial y}-2M_{xy}^b\frac{\partial^2\delta w_0}{\partial x\partial y}\\ +k_1A'M_{xy}^s\frac{\partial^2\delta\theta}{\partial x\partial y}+N_{xy}\frac{\partial\delta v_0}{\partial x}\\ +k_2B'M_{xy}^s\frac{\partial^2\delta\theta}{\partial x\partial y}+k_2B'Q_{yz}^s\frac{\partial\delta\theta}{\partial y}\\ +S_{yz}^s\frac{\partial\delta\theta}{\partial y}+k_1A'Q_{xz}^s\frac{\partial\delta\theta}{\partial x}\\ +S_{xz}^s\frac{\partial\delta\theta}{\partial x}\end{bmatrix}dxdy, \quad (28)$$

where *N*, *M*, *S*, and *Q* are the force and moment components represented in the following forms [30]:

$$\left(N_i,M_i^b,M_i^s\right)=\int_{-\frac{h}{2}}^{+\frac{h}{2}}\big(1,z,f(z)\big)\,\sigma_i dz,\ (i=x,y,xy), \quad (29)$$

$$N_z=\int_{-\frac{h}{2}}^{+\frac{h}{2}}\sigma_z dz, \quad (30)$$

$$\left(S_{xz}^s,S_{yz}^s\right)=\int_{-\frac{h}{2}}^{+\frac{h}{2}}\left(\tau_{xz},\tau_{yz}\right)g(z)dz, \quad (31)$$

$$\left(Q_{xz}^s,Q_{yz}^s\right)=\int_{-\frac{h}{2}}^{+\frac{h}{2}}\left(\tau_{xz},\tau_{yz}\right)f'(z)dz. \quad (32)$$

Using Eqs. (16)-(22), and (24), *N*, *M*, *S*, and *Q* can be represented (see Appendix A).

The effective temperature-dependent stiffness elements are stated as follows:

$$\begin{Bmatrix}A_{11}&B_{11}&D_{11}&B_{11}^s&D_{11}^s&H_{11}^s\\ A_{12}&B_{12}&D_{12}&B_{12}^s&D_{12}^s&H_{12}^s\\ A_{66}&B_{66}&D_{66}&B_{66}^s&D_{66}^s&H_{66}^s\end{Bmatrix}=\int_{-h/2}^{h/2}[1,z,z^2,f(z),zf(z),f^2(z)]\begin{Bmatrix}C_{11}(z,T)\\ C_{12}(z,T)\\ C_{66}(z,T)\end{Bmatrix}dz. \quad (33)$$

$$(A_{22},B_{22},D_{22},B_{22}^s,D_{22}^s,H_{22}^s)=(A_{11},B_{11},D_{11},B_{11}^s,D_{11}^s,H_{11}^s), \quad (34)$$

$$\begin{Bmatrix}L\\ L^a\\ R\end{Bmatrix}=\int_{-\frac{h}{2}}^{\frac{h}{2}}C_{ij}(z,T)\begin{Bmatrix}1\\ z\\ f(z)\end{Bmatrix}g'(z)dz,\{R^a\}=\int_{-h/2}^{h/2}C_{33}(z,T)\,[g'(z)]^2\,dz \text{ and } (i=1,2\,;j=3), \quad (35)$$

$$F_{44}^s=F_{55}^s=\int_{-h/2}^{h/2}C_{ii}(z,T)[\,f'(z)]^2\ dz \text{ and } (i=4,5), \quad (36)$$

$$X_{44}^s=X_{55}^s=\int_{-h/2}^{h/2}C_{ii}(z,T)\,f(z)g(z)\ dz \text{ and } (i=4,5), \quad (37)$$

$$A_{44}^s=A_{55}^s=\int_{-h/2}^{h/2}C_{ii}(z,T)\,[g(z)]^2\ dz \text{ and } (i=4,5). \quad (38)$$

The variation of the potential energy of foundations is given by:

$$\delta P_f=\int_0^a\int_0^b(f_e+f_{Kerr})\delta w_0\,dxdy, \quad (39)$$

where f_e and f_{Kerr} are the densities of reaction forces for the Pasternak foundation and Keer foundation model, respectively.

Importantly, the Pasternak foundation is a two-parameter elastic model and its distributed reaction force is expressed as:

$$f_e=K_w w_0-K_p\left(\frac{\partial^2 w_0}{\partial x^2}+\frac{\partial^2 w_0}{\partial y^2}\right), \quad (40)$$

in which K_w and K_p are the Winkler and the shear layer coefficients of the elastic foundation, respectively.

More importantly, the Kerr model foundation is a three-parameter elastic model, and its distributed reaction force is expressed as:

$$f_{Kerr}=\left(\frac{K_l K_u}{K_l+K_u}\right)w_0-\left(\frac{K_s K_u}{K_l+K_u}\right)\left(\frac{\partial^2 w_0}{\partial x^2}+\frac{\partial^2 w_0}{\partial y^2}\right), \tag{41}$$

in which K_s is the shear layer parameter, K_u is the upper elastic layer, and K_l is the lower elastic layer.

The kinetic energy variation is represented as you can see in Box I, Mamen [30].

The dot–superscript convention is used to denote the time derivative.

$I_0, I_1, I_2, J_1, J_2, K_2, J_0$ and K_0 are the independent–temperature mass inertias as you can see in Eq. (44):

$$[I_0, I_1, I_2, J_1, J_2, K_2, J_0, K_0]=\int_{-\frac{h}{2}}^{+\frac{h}{2}}\rho(z)[1, z, z^2, f(z), zf(z), f^2(z), g(z),^2(z)]\,dz. \tag{44}$$

The variation of work done by thermal loads is written in the following form:

$$\delta V=\int_0^a\int_0^b\left(N_x^T\frac{\partial^2 w}{\partial x^2}+2N_{xy}^T\frac{\partial^2 w}{\partial x\partial y}+N_y^T\frac{\partial^2 w}{\partial y^2}\right)\delta w\,dxdy, \tag{45}$$

where N_x^T, N_y^T, and N_{xy}^T are defined as follows:

$$N_x^T=\int_{-h/2}^{+h/2}C_{11}(z,T)\,\alpha(z,T)(T(z)-T_0)dz, \tag{46}$$

$$N_y^T=\int_{-h/2}^{+h/2}C_{22}(z,T)\,\alpha(z,T)(T(z)-T_0)dz, \tag{47}$$

$$N_{xy}^T=\int_{-h/2}^{+h/2}C_{12}(z,T)\,\alpha(z,T)(T(z)-T_0)dz, \tag{48}$$

As $C_{11}=C_{22}$, we get $N_x^T=N_y^T=N^T$.

The variation of work done by thermal loads becomes as follows:

$$\delta V=\int_0^a\int_0^b\left(N^T\left(\frac{\partial^2 w}{\partial x^2}+\frac{\partial^2 w}{\partial y^2}\right)+2N_{xy}^T\frac{\partial^2 w}{\partial x\partial y}\right)\delta w dxdy, \tag{49}$$

where $T(z)$ is the nonlinear field of temperature (see Eqs. (5)-(7), and the initial temperature T_0 = 300 K.

Substituting Eqs. (28), (39), (43), and (49) into Eq. (25), the equations of motion are obtained in the Box II:

$$\delta K=\int_0^a\int_0^b\int_{-\frac{h}{2}}^{+\frac{h}{2}}\rho(z)(\dot{u}_0\delta\dot{u}_0+\dot{v}_0\delta\dot{v}_0+\dot{w}_0\delta\dot{w}_0)\,dxdydz, \tag{42}$$

$$\delta K=\int_0^a\int_0^b\begin{bmatrix}I_0(\dot{u}_0\delta\dot{u}_0+\dot{v}_0\delta\dot{v}_0+\dot{w}_0\delta\dot{w}_0)-I_1\left(\dot{u}_0\frac{\partial\delta\dot{w}_0}{\partial x}+\frac{\partial\dot{w}_0}{\partial x}\delta\dot{u}_0+\dot{v}_0\frac{\partial\delta\dot{w}_0}{\partial y}+\frac{\partial\dot{w}_0}{\partial y}\delta\dot{v}_0\right)\\+I_2\left(\frac{\partial\dot{w}_0}{\partial x}\frac{\partial\delta\dot{w}_0}{\partial x}+\frac{\partial\dot{w}_0}{\partial y}\frac{\partial\delta\dot{w}_0}{\partial y}\right)\\+J_1\left(k_1A'\dot{u}_0\frac{\partial\delta\dot{\theta}}{\partial x}+k_1A'\frac{\partial\dot{\theta}}{\partial x}\delta\dot{u}_0+k_2B'\dot{v}_0\frac{\partial\delta\dot{\theta}}{\partial y}+k_2B'\frac{\partial\dot{\theta}}{\partial y}\delta\dot{v}_0\right)\\-J_2\left(k_1A'\frac{\partial\dot{w}_0}{\partial x}\frac{\partial\delta\dot{\theta}}{\partial x}+k_1A'\frac{\partial\dot{\theta}}{\partial x}\frac{\partial\delta\dot{w}_0}{\partial x}+k_2B'\frac{\partial\dot{w}_0}{\partial y}\frac{\partial\delta\dot{\theta}}{\partial y}+k_2B'\frac{\partial\dot{\theta}}{\partial y}\frac{\partial\delta\dot{w}_0}{\partial y}\right)\\+K_2\left[(k_1A')^2\frac{\partial\dot{\theta}}{\partial x}\frac{\partial\delta\dot{\theta}}{\partial x}+(k_2B')^2\frac{\partial\dot{\theta}}{\partial y}\frac{\partial\delta\dot{\theta}}{\partial y}\right]+J_0(\dot{w}_0\delta\dot{\theta}+\dot{\theta}\delta\dot{w}_0)+K_0\dot{\theta}\delta\dot{\theta}\end{bmatrix}dxdy. \tag{43}$$

Box I

$$\delta u_0:\frac{\partial N_x}{\partial x}+\frac{\partial N_{xy}}{\partial y}=I_0\ddot{u}_0-I_1\frac{\partial\ddot{w}_0}{\partial x}+J_1k_1A'\frac{\partial\ddot{\theta}}{\partial x}, \tag{50}$$

$$\delta v_0:\frac{\partial N_y}{\partial y}+\frac{\partial N_{xy}}{\partial x}=I_0\ddot{v}_0-I_1\frac{\partial\ddot{w}_0}{\partial y}+J_1k_2B'\frac{\partial\ddot{\theta}}{\partial y}, \tag{51}$$

$$\begin{aligned}\delta w_0:&\frac{\partial^2 M_x^b}{\partial x^2}+\frac{\partial^2 M_y^b}{\partial y^2}+2\frac{\partial^2 M_{xy}^b}{\partial x\partial y}-(f_e+f_{Kerr})+N^T\left(\frac{\partial^2 w_0}{\partial x^2}+\frac{\partial^2 w_0}{\partial y^2}\right)+N^Tg(0)\left(\frac{\partial^2\theta}{\partial x^2}+\frac{\partial^2\theta}{\partial y^2}\right)+2{N_{xy}}^T\left(\frac{\partial^2 w_0}{\partial x\partial y}\right)\\&+N^Tg(0)\left(\frac{\partial^2\theta}{\partial x\partial y}\right)=I_0\ddot{w}_0+I_1\left(\frac{\partial\ddot{u}_0}{\partial x}+\frac{\partial\ddot{v}_0}{\partial y}\right)-I_2\left(\frac{\partial^2\ddot{w}_0}{\partial x^2}+\frac{\partial^2\ddot{w}_0}{\partial y^2}\right)+J_2\left(k_1A^{\frac{\partial^2\ddot{\theta}}{\partial x^2}}+k_2B^{\frac{\partial^2\ddot{\theta}}{\partial y^2}}\right)+J_0\ddot{\theta},\end{aligned} \tag{52}$$

$$\begin{aligned}\delta\theta:&-k_1A'\frac{\partial^2 M_x^s}{\partial x^2}-k_2B'\frac{\partial^2 M_y^s}{\partial y^2}-N_z+(k_1A'+k_2B')\frac{\partial^2 M_{xy}^s}{\partial x\partial y}+k_1A'\frac{\partial Q_{xz}^s}{\partial x}+k_2B'\frac{\partial Q_{yz}^s}{\partial y}+\frac{\partial S_{xz}^s}{\partial x}+\frac{\partial S_{yz}^s}{\partial y}+N^Tg(0)\left(\frac{\partial^2 w_0}{\partial x^2}+\frac{\partial^2 w_0}{\partial y^2}\right)\\&+N^Tg(0)^2\left(\frac{\partial^2\theta}{\partial x^2}+\frac{\partial^2\theta}{\partial y^2}\right)+2{N_{xy}}^Tg(0)\left(\frac{\partial^2 w_0}{\partial x\partial y}\right)+N^Tg(0)^2\left(\frac{\partial^2\theta}{\partial x\partial y}\right)=-J_1\left(k_1A'\frac{\partial\ddot{u}_0}{\partial x}+k_2B'\frac{\partial\ddot{v}_0}{\partial y}\right)+J_2\left(k_1A'\frac{\partial^2\ddot{w}_0}{\partial x^2}+k_2B'\frac{\partial^2\ddot{w}_0}{\partial y^2}\right)\\&-K_2\left[(k_1A')^2\frac{\partial^2\ddot{\theta}}{\partial x^2}+(k_2B')^2\frac{\partial^2\ddot{\theta}}{\partial y^2}\right]+J_0\ddot{w}_0+K_0\ddot{\theta}.\end{aligned} \tag{53}$$

Box II

Eqs. (50)-(53) can be expressed in terms of u_0, v_0, w_0, and θ by using Eq. (33) as we can see in Box III.

4.3. Analytical solutions for FGM plate

We are interested here in finding exact solutions for the free vibration problem of simply-supported FG plate. With the Navier solution technique, the change in displacement can be calculated as follows:

$$u_0(x,y,t) = \sum_{m=1}^{\infty}\sum_{n=1}^{\infty} u_{mn}\cos(\lambda x)\sin(\beta y)\, e^{i\omega_n t}, \tag{58}$$

$$v_0(x,y,t) = \sum_{m=1}^{\infty}\sum_{n=1}^{\infty} v_{mn}\sin(\lambda x)\cos(\beta y)\, e^{i\omega_n t}, \tag{59}$$

$$w_0(x,y,t) = \sum_{m=1}^{\infty}\sum_{n=1}^{\infty} w_{mn}\sin(\lambda x)\sin(\beta y)\, e^{i\omega_n t}, \tag{60}$$

$$\theta(x,y,t) = \sum_{m=1}^{\infty}\sum_{n=1}^{\infty} \theta_{mn}\sin(\lambda x)\sin(\beta y)\, e^{i\omega_n t}, \tag{61}$$

$$\text{with } \lambda = \frac{m\pi}{a}, \text{ and } \beta = \frac{n\pi}{b}, \tag{62}$$

in which u_{mn},v_{mn},w_{mn}, and θ_{mn} are unknown parameters to be determined. The boundary conditions are represented as:

$$v_0 = w_0 = \theta = \frac{\partial\theta}{\partial y} = N_x = M_x^b = M_x^s = 0 \text{at} x = 0, a, \tag{63}$$

$$u_0 = w_0 = \theta = \frac{\partial\theta}{\partial x} = N_y = M_y^b = M_y^s = 0 \text{at} y = 0, b. \tag{64}$$

Substituting Eq. (58)-(61) into Eqs. (50)-(53), respectively, leads to the Eqs. (65)-(68) are shown in Box IV.

By finding the determinant of the coefficient matrix of the above equations and setting this multinomial to zero, we can find natural frequencies ω_n:

$$det\begin{bmatrix} d_{11} & d_{12} & d_{13} & d_{14} \\ d_{21} & d_{22} & d_{23} & d_{24} \\ d_{31} & d_{32} & d_{33} & d_{34} \\ d_{41} & d_{42} & d_{43} & d_{44}\end{bmatrix} = 0, \tag{69}$$

where the different components of the previous matrix are presented in Appendix B.

5. Findings and discussion

Evaluations are made with analytical and numerical results published by various researchers. Additionally, the solutions in the tables and graphs are revealed in non-dimensional formulas that are proposed as follows:

$$\begin{aligned}\delta u_0:\ & A_{11}\frac{\partial^2 u_0}{\partial x^2} + A_{66}\frac{\partial^2 u_0}{\partial y^2} + (A_{12}+A_{66})\frac{\partial^2 v_0}{\partial x\partial y} - B_{11}\frac{\partial^3 w_0}{\partial x^3} - (B_{12}+2B_{66})\frac{\partial^3 w_0}{\partial x\partial y^2} + [B_{12}^s k_2 B' + B_{66}^s(k_1A' + k_2B')]\frac{\partial^3\theta}{\partial x\partial y^2} \\ & + B_{11}^s k_1 A'\frac{\partial^3\theta}{\partial x^3} + L\frac{\partial\theta}{\partial x} = I_0\ddot{u}_0 - I_1\frac{\partial\ddot{w}_0}{\partial x} + J_1 k_1 A'\frac{\partial\ddot{\theta}}{\partial x},\end{aligned} \tag{54}$$

$$\begin{aligned}\delta v_0:\ & (A_{12}+A_{66})\frac{\partial^2 u_0}{\partial x\partial y} + A_{22}\frac{\partial^2 v_0}{\partial y^2} + A_{66}\frac{\partial^2 v_0}{\partial x^2} - B_{22}\frac{\partial^3 w_0}{\partial y^3} - (B_{12}+2B_{66})\frac{\partial^3 w_0}{\partial x^2\partial y} + [B_{12}^s k_1 A' + B_{66}^s(k_1A' + k_2B')]\frac{\partial^3\theta}{\partial x^2\partial y} \\ & + B_{22}^s k_2 B'\frac{\partial^3\theta}{\partial y^3} + L\frac{\partial\theta}{\partial y} = I_0\ddot{v}_0 - I_1\frac{\partial\ddot{w}_0}{\partial y} + J_1 k_2 B'\frac{\partial\ddot{\theta}}{\partial y},\end{aligned} \tag{55}$$

$$\begin{aligned}\delta w_0:\ & B_{11}\frac{\partial^3 u_0}{\partial x^3} + (B_{12}+2B_{66})\frac{\partial^3 u_0}{\partial x\partial y^2} + (B_{12}+2B_{66})\frac{\partial^3 v_0}{\partial x^2\partial y} + B_{22}\frac{\partial^3 v_0}{\partial y^3} + 2(D_{12}+2D_{66})\frac{\partial^4 w_0}{\partial x^2\partial y^2} - D_{22}\frac{\partial^4 w_0}{\partial y^4} - D_{11}\frac{\partial^4 w_0}{\partial x^4} \\ & + D_{11}^s k_1 A'\frac{\partial^4\theta}{\partial x^4} - [(D_{12}^s + 2D_{66}^s)(k_1A' + k_2B')]\frac{\partial^4\theta}{\partial x^2\partial y^2} + D_{22}^s k_2 B'\frac{\partial^4\theta}{\partial y^4} + L_a\left(\frac{\partial^2\theta}{\partial x^2} + \frac{\partial^2\theta}{\partial y^2}\right) - K_w w_0 + K_p\left(\frac{\partial^2 w_0}{\partial x^2} + \frac{\partial^2 w_0}{\partial y^2}\right) \\ & - \left(\frac{K_l K_u}{K_l + K_u} w_0\right) + \left(\frac{K_s K_u}{K_l + K_u}\right)\left(\frac{\partial^2 w_0}{\partial x^2} + \frac{\partial^2 w_0}{\partial y^2}\right) + N^T\left(\frac{\partial^2 w_0}{\partial x^2} + \frac{\partial^2 w_0}{\partial y^2}\right) + N^T g(0)\left(\frac{\partial^2\theta}{\partial x^2} + \frac{\partial^2\theta}{\partial y^2}\right) + 2{N_{xy}}^T\left(\frac{\partial^2 w_0}{\partial x\partial y}\right) \\ & + 2{N_{xy}}^T g(0)\left(\frac{\partial^2\theta}{\partial x\partial y}\right) = I_0\ddot{w}_0 + I_1\left(\frac{\partial\ddot{u}_0}{\partial x} + \frac{\partial\ddot{v}_0}{\partial y}\right) - I_2\left(\frac{\partial^2\ddot{w}_0}{\partial x^2} + \frac{\partial^2\ddot{w}_0}{\partial y^2}\right) + J_2\left(k_1A'\frac{\partial^2\ddot{\theta}}{\partial x^2} + k_2B'\frac{\partial^2\ddot{\theta}}{\partial y^2}\right) + J_0\ddot{\theta},\end{aligned} \tag{56}$$

$$\begin{aligned}\delta\theta:\ & -B_{11}^s k_1 A'\frac{\partial^3 u_0}{\partial x^3} - [B_{12}^s k_2 B' + B_{66}^s(k_1A' + k_2B')]\frac{\partial^3 u_0}{\partial x\partial y^2} - [B_{12}^s k_1 A' + B_{66}^s(k_1A' + k_2B')]\frac{\partial^3 v_0}{\partial x^2\partial y} - B_{22}^s k_2 B'\frac{\partial^3 v_0}{\partial y^3} \\ & + D_{11}^s k_1 A'\frac{\partial^4 w_0}{\partial x^4} + [(D_{12}^s + 2D_{66}^s)(k_1A' + k_2B')]\frac{\partial^4 w_0}{\partial x^2\partial y^2} + D_{22}^s k_2 B'\frac{\partial^4 w_0}{\partial y^4} - H_{11}^s(k_1A')^2\frac{\partial^4\theta}{\partial x^4} - H_{22}^s(k_2B')^2\frac{\partial^4\theta}{\partial y^4} \\ & - [2H_{12}^s k_1A' k_2B' + (k_1A' + k_2B')^2 H_{66}^s]\frac{\partial^4\theta}{\partial x^2\partial y^2} - [2Rk_1A' - F_{55}^s(k_1A')^2 - 2X_{55}^s k_1A' - A_{55}^s]\frac{\partial^2\theta}{\partial x^2} \\ & - [2Rk_2B' - F_{44}^s(k_2B')^2 - 2X_{44}^s k_2B' - A_{44}^s]\frac{\partial^2\theta}{\partial y^2} + L_a\left(\frac{\partial^2 w_0}{\partial x^2} + \frac{\partial^2 w_0}{\partial y^2}\right) - L\left(\frac{\partial u_0}{\partial x} + \frac{\partial v_0}{\partial y}\right) - R_a\theta + N^T g(0)\left(\frac{\partial^2 w_0}{\partial x^2} + \frac{\partial^2 w_0}{\partial y^2}\right) \\ & + N^T g(0)^2\left(\frac{\partial^2\theta}{\partial x^2} + \frac{\partial^2\theta}{\partial y^2}\right) + 2{N_{xy}}^T g(0)\left(\frac{\partial^2 w_0}{\partial x\partial y}\right) + 2{N_{xy}}^T g(0)^2\left(\frac{\partial^2\theta}{\partial x\partial y}\right) = -J_1\left(k_1A'\frac{\partial\ddot{u}_0}{\partial x} + k_2B'\frac{\partial\ddot{v}_0}{\partial y}\right) \\ & + J_2\left(k_1A'\frac{\partial^2\ddot{w}_0}{\partial x^2} + k_2B'\frac{\partial^2\ddot{w}_0}{\partial y^2}\right) - K_2\left[(k_1A')^2\frac{\partial^2\ddot{\theta}}{\partial x^2} + (k_2B')^2\frac{\partial^2\ddot{\theta}}{\partial y^2}\right] + J_0\ddot{w}_0 + K_0\ddot{\theta},\end{aligned} \tag{57}$$

Box III.

$$[-A_{11}\lambda^2 - A_{66}\beta^2 - I_0\omega_n{}^2]u_{mn} + [-(A_{11}+A_{66})\lambda\beta]v_{mn} + [B_{11}\lambda^3 + (B_{12}+2B_{66})\lambda\beta^2 + I_1\omega_n{}^2\lambda]w_{mn}$$
$$+\left[-k_1A'J_1\lambda\omega_n{}^2 - \left(B_{12}^s k_2 B' + B_{66}^s(k_1A' + k_2B')\right)\lambda\beta^2 - B_{11}^s k_1 A'\lambda^3 + L\lambda\right]\theta_{mn} = 0, \quad (65)$$

$$[-(A_{12}+A_{66})\lambda\beta]u_{mn} + [-A_{22}\beta^2 - A_{66}\lambda^2 - I_0\omega_n{}^2]v_{mn} + [I_1\omega_n{}^2\beta + B_{22}\beta^3 + (B_{12}+2B_{66})\lambda^2\beta]w_{mn}$$
$$+\left[-k_2B'J_1\beta\omega_n{}^2 - \left(B_{12}^s k_1 A' + B_{66}^s(k_1A' + k_2B')\right)\beta\lambda^2 - B_{22}^s k_2 B'\beta^3 + L\beta\right]\theta_{mn} = 0, \quad (66)$$

$$[I_1\omega_n{}^2\lambda + B_{11}\lambda^3 + (B_{12}+2B_{66})\lambda\beta^2]u_{mn} + [I_1\omega_n{}^2\beta + B_{22}\beta^3 + (B_{12}+2B_{66})\lambda^2\beta]v_{mn}$$
$$+\begin{bmatrix} -\omega_n{}^2\left(I_0 + I_2(\lambda^2+\beta^2)\right) - 2(D_{12}+2D_{66})\lambda^2\beta^2 - D_{22}\beta^4 - D_{11}\lambda^4 \\ -K_w - K_p(\lambda^2+\beta^2) - \left(\dfrac{K_lK_u}{K_l+K_u}\right) - \left(\dfrac{K_sK_u}{K_l+K_u}\right)(\lambda^2+\beta^2) + N^T(\lambda^2+\beta^2) - 2N_{xy}{}^T(\lambda\beta) \end{bmatrix} w_{mn}$$
$$+\begin{bmatrix} -\omega_n{}^2(-J_2(k_1A'\lambda^2 + k_2B'\beta^2) + J_0) + D_{11}^s k_1A'\lambda^4 + (D_{12}^s + 2D_{66}^s)(k_1A' + k_2B')\lambda^2\beta^2 \\ +D_{22}^s k_2B'\beta^4 - L_a(\lambda^2+\beta^2) + N^T g(0)(\lambda^2+\beta^2) - 2N_{xy}{}^T g(0)(\lambda\beta) \end{bmatrix}\theta_{mn} = 0, \quad (67)$$

$$\left[-k_1A'J_1\lambda\omega_n{}^2 - \left(B_{12}^s k_2B' + B_{66}^s(k_1A' + k_2B')\right)\lambda\beta^2 - B_{11}^s k_1A'\lambda^3 + L\lambda\right]u_{mn}$$
$$+\left[-k_2B'J_1\beta\omega_n{}^2 - \left(B_{12}^s k_1A' + B_{66}^s(k_1A' + k_2B')\right)\beta\lambda^2 - B_{22}^s k_2B'\beta^3 + L\beta\right]v_{mn}$$
$$+\begin{bmatrix} -\omega_n{}^2(-J_2(k_1A'\lambda^2 + k_2B'\beta^2) + J_0) + D_{11}^s k_1A'\lambda^4 + (D_{12}^s + 2D_{66}^s)(k_1A' + k_2B')\lambda^2\beta^2 \\ +D_{22}^s k_2B'\beta^4 - L_a(\lambda^2+\beta^2) + g(0)N^T(\lambda^2+\beta^2) - 2N_{xy}{}^T g(0)(\lambda\beta) \end{bmatrix} w_{mn}$$
$$+\begin{bmatrix} -\omega_n{}^2(K_2((k_1A')^2\lambda^2 + (k_2B')^2\beta^2) + K_0) - (k_1A')^2H_{11}^s\lambda^4 - (k_2B')^2H_{22}^s\beta^4 \\ -(2H_{12}^s k_1A'k_2B' + H_{66}^s(k_1A' + k_2B')^2)\lambda^2\beta^2 \\ +(-F_{55}^s(k_1A')^2 + 2k_1A'R - 2k_1A'X_{55}^s - A_{55}^s)\lambda^2 \\ +(-F_{44}^s(k_2B')^2 + 2k_2B'R - 2k_2B'X_{44}^s - A_{44}^s)\beta^2 - R_a + N^T g(0)^2(\lambda^2+\beta^2) - 2N_{xy}{}^T g(0)^2(\lambda\beta) \end{bmatrix}\theta_{mn} = 0. \quad (68)$$

Box IV.

Table 2. Comparison of 3D fundamental frequencies $\bar{\beta}$ for square FG plate Al_2/AlO_3 with $E_c = 380$ GPa, $E_m = 70$ GPa , $\rho_c = 3800\ \frac{kg}{m^3}$, $\rho_m = 2702\ \frac{kg}{m^3}$ and $\nu_c = \nu_m = 0{,}3$.

a/h	Mode N°(m, n)	Source	*k*				
			0	0.5	1	4	10
5	1 (1, 1)	Zaoui et al. [28]-5v	0.2126	0.1829	0.1663	0.1411	0.1320
		Present (quasi-3D) -4v	0.2127	0.1832	0.1663	0.1410	0.1321
	2 (1, 2)	Zaoui et al. [28]-5v	0.4674	0.4052	0.3687	0.3052	0.2817
		Present (quasi-3D) -4v	0.4674	0.4058	0.3687	0.3049	0.2817
	3 (2, 2)	Zaoui et al. [28]-5v	0.6783	0.5911	0.5381	0.4389	0.4018
		Present (quasi-3D) -4v	0.6778	0.5914	0.5377	0.4383	0.4014
10	1 (1, 1)	Zaoui et al. [28]-5v	0.0579	0.0495	0.0450	0.0390	0.0369
		Present (quasi-3D) -4v	0.0578	0.0495	0.0449	0.0389	0.0369
	2 (1, 2)	Zaoui et al. [28]-5v	0.1383	0.1186	0.1078	0.0924	0.0868
		Present (quasi-3D) -4v	0.1384	0.1188	0.1079	0.0923	0.0869
	3 (2, 2)	Zaoui et al. [28]-5v	0.2126	0.1829	0.1663	0.1411	0.1320
		Present (quasi-3D) -4v	0.2127	0.1832	0.1663	0.1410	0.1321
20	1 (1, 1)	Zaoui et al. [28]-5v	0.0148	0.0126	0.0115	0.0100	0.0095
		Present (quasi-3D) -4v	0.0148	0.0126	0.0115	0.0100	0.0095

4v: Four variables, 5v: Five variables.

$$\bar{\beta} = \omega_n h\sqrt{\frac{\rho_c}{E_c}}, \quad (70)$$

$$\bar{\psi} = \omega_n h\sqrt{\frac{\rho_m}{E_m}}, \quad (71)$$

$$\bar{\omega} = \omega_n\left(\frac{a^2}{h}\right)\sqrt{\frac{\rho_0(1-\nu_0{}^2)}{E_0}}, \quad (72)$$

where: $\nu_0 = 0.28$:

$$K_w = \frac{k_wD_0}{a^4}\ K_p = \frac{k_pD_0}{a^2}, \quad (73)$$

$$K_l = \frac{k_lD_0}{a^4}\ K_u = \frac{k_uD_0}{a^4}\ K_s = \frac{k_sD_0}{a^2}, \quad (74)$$

where: $D_0 = \frac{E_0h^3}{12(1-\nu^2)}$,

ρ_0 and E_0 are the parameters of metal at ambient temperature (300 K).

The proposed shear deformation theory results, based on four variables, are verified in Table 2 by comparing the fundamental frequencies of FG square plates Al_2/AlO_3 with the exact results published by Zaoui et al. [28] using five variables. Furthermore, the fundamental frequencies are given for different slenderness ratios (a/h=5, 10, and 20) and the first three modes. The comparison concludes that the proposed theory functions correctly and matches the results previously published by Zaoui et al. [28].

Additionally, the proposed theory's results are compared with those published by Zaoui et al. [28] and Mengzhen et al. [39] for FG square plates Al_2/AlO_3 lying on elastic foundations by considering different power-law indexes (see Tables 3 and 4).

Finally, the fundamental frequencies of FG plates composed of (Si_3N_4-SUS304) are compared with those published by Huang and Shen [3]; Parida and Mohanty [6], and Zaoui et al. [19] for (a/h=5 and 20) (see Table 5). Calculations are performed for these FG plates with the subsequent properties: a/b=1, a=8 h, ρ_c=2770 kg/m^3, ρ_m=8166 kg/m^3, and v_c= v_m=0.28, K_c=9.19 W/mK, and K_m=12.04 W/mK. Importantly, the present results reported in Table 5 agree satisfactorily with the published ones. The present method can successfully calculate the 3D dynamic response of FG plates exposed to NLTR.

As mentioned in Figure 2, the thermal conductivity will be considered temperature-dependent to meet the required results. Notably, the examination of Table 6 reveals that the natural frequencies in temperature-dependent are lower than those in temperature-independent plates.

Variations of fundamental frequencies of the FGM plates lying on Winkler/Pasternak and Kerr foundations at different temperatures on the ceramic side are shown in Tables 7 and 8, wherein the first five modes of free vibration are presented. The fundamental frequencies are evaluated for different k. The temperature of the bottom side is kept constant at T_m= 300 K, while two different temperatures of the top side are considered with a rise of 100 and 300 K from reference temperature (T_0=300 K).

Table 3. Comparison of first 3D fundamental frequencies $\bar{\psi}$ for square Al_2/AlO_3 plate lying on Winkler/Pasternak foundation.

(k_w, k_p)	h/a	Source	k = 0	0.5	1	2	5
(0, 100)	0.05	Zaoui et al. [28]-5v	0.0406	0.0387	0.0380	0.0376	0.0378
		Present (quasi-3D) -4v	0.0406	0.0387	0.0379	0.0376	0.0378
	0.1	Zaoui et al. [28]-5v	0.1594	0.1525	0.1497	0.1483	0.1489
		Present (quasi-3D) -4v	0.1595	0.1527	0.1498	0.1483	0.1489
	0.2	Zaoui et al. [28]-5v	0.6015	0.5795	0.5701	0.5652	0.5662
		Present (quasi-3D) -4v	0.6036	0.5828	0.5730	0.5671	0.5674
(100, 0)	0.05	Zaoui et al. [28]-5v	0.0298	0.0257	0.0236	0.0219	0.0208
		Present (quasi-3D) -4v	0.0298	0.0257	0.0236	0.0218	0.0208
	0.1	Zaoui et al. [28]-5v	0.1164	0.1007	0.0924	0.0854	0.0809
		Present (quasi-3D) -4v	0.1164	0.1008	0.0924	0.0853	0.0809
	0.2	Zaoui et al. [28]-5v	0.4290	0.3737	0.3433	0.3161	0.2948
		Present (quasi-3D) -4v	0.4293	0.3745	0.3436	0.3156	0.2948
(100, 100)	0.05	Zaoui et al. [28]-5v	0.0411	0.0393	0.0386	0.0383	0.0385
		Present (quasi-3D) -4v	0.0410	0.0393	0.0386	0.0383	0.0385
	0.1	Zaoui et al. [28]-5v	0.1614	0.1548	0.1522	0.1509	0.1517
		Present (quasi-3D) -4v	0.1614	0.1549	0.1522	0.1509	0.1517
	0.2	Zaoui et al. [28]-5v	0.6093	0.5884	0.5797	0.5754	0.5770
		Present (quasi-3D) -4v	0.6115	0.5918	0.5827	0.5774	0.5784

4v: Four variables, 5v: Five variables.

Table 4. Comparaison of first 3D fundamental frequencies $\bar{\psi}$ for square Al_2/AlO_3 plate lying on Kerr foundation.

(k_u, k_s)	h/a	Source	k = 0	0.5	1	2	5
(100, 0)	0.05	Mengzhen et al. [39]-5v	0.0294	0.0253	0.0231	0.0212	0.0202
		Present (quasi-3D) -4v	0.0294	0.0253	0.0231	0.0212	0.0202
	0.1	Mengzhen et al. [39]-5v	0.1149	0.0988	0.0903	0.0830	0.0783
		Present (quasi-3D) -4v	0.1150	0.0990	0.0904	0.0830	0.0783
	0.2	Mengzhen et al. [39]-5v	0.4225	0.3659	0.3345	0.3059	0.2837
		Present (quasi-3D) -4v	0.4237	0.3673	0.3353	0.3060	0.2839
(100, 100)	0.05	Mengzhen et al. [39]-5v	0.0356	0.0329	0.0316	0.0307	0.0305
		Present (quasi-3D) -4v	0.0356	0.0329	0.0316	0.0307	0.0305
	0.1	Mengzhen et al. [39]-5v	0.1395	0.1292	0.1243	0.1210	0.1198
		Present (quasi-3D) -4v	0.1396	0.1293	0.1244	0.1210	0.1198
	0.2	Mengzhen et al. [39]-5v	0.5218	0.4873	0.4705	0.4580	0.4522
		Present (quasi-3D) -4v	0.5237	0.4898	0.4724	0.4589	0.4522

4v: Four variables, 5v: Five variables.

Table 5. Comparaison of first fundamental frequencies $\bar{\omega}$ for Si_3N_4-SUS304 square plates in nonlinear thermal environments with a/b=1 and a=8 h.

T	k	Present (quasi-3D)	Present (2D)	Huang and Shen [3]-2D	Parida and Mohanty [6]-2D	Zaoui et al. [19]-2D
T_c=300 K T_m=300 K	Si_3N_4	12.537	12.503	12.495	12.587	12.508
	0.5	8.640	8.607	8.675	9.094	8.610
	1.0	7.572	7.542	7.555	7.656	7.545
	2.0	6.791	6.769	6.777	6.78	6.771
	SUS304	5.425	5.410	5.405	5.445	5.411
T_c=400 K T_m=300 K	Si_3N_4	12.332	12.299	12.397	12.387	12.308
	0.5	8.514	8.483	8.615	8.615	8.454
	1.0	7.468	7.440	7.474	7.51	7.399
	2.0	6.701	6.680	6.693	6.642	6.632
	SUS304	5.318	5.304	5.311	5.311	5.279
T_c=600 K T_m=300 K	Si_3N_4	11.932	11.901	11.984	11.971	11.887
	0.5	8.266	8.236	8.269	8.272	8.119
	1.0	7.260	7.235	7.171	7.186	7.082
	2.0	6.522	6.503	6.398	6.327	6.323
	SUS304	4.979	4.964	4.971	4.989	4.945

Table 6. 3D fundamental frequencies $\bar{\omega}$ for Si_3N_4-SUS304 square plates in thermal environments with a/b=1 and a=8 h.

T	k	Modes				
		(1, 1)	(1, 2)	(2, 2)	(1, 3)	(2, 3)
T_c=300 K T_m=300 K	Si_3N_4	12.411	29.147	44.196	53.498	66.566
	0.5	8.637	20.270	30.718	37.170	46.228
	1.0	7.601	17.785	26.882	32.373	40.188
	2.0	6.836	15.986	24.157	29.185	36.224
	SUS304	5.495	12.873	19.469	23.530	29.216
T_c=400 K T_m=300 K Temperature dependent	Si_3N_4	12.204	28.757	43.655	52.843	65.786
	0.5	8.510	20.049	30.425	36.813	45.814
	1.0	7.490	17.555	26.454	31.810	39.200
	2.0	6.746	15.844	23.986	28.974	35.995
	SUS304	5.395	12.709	19.270	23.275	28.939
T_c=400 K T_m=300 K Temperature independent	Si_3N_4	12.336	29.061	44.114	53.398	66.475
	0.5	8.5734	20.197	30.648	37.084	46.151
	1.0	7.540	17.702	26.815	32.233	40.015
	2.0	6.777	15.915	24.091	29.099	36.149
	SUS304	5.434	12.797	19.401	23.436	29.138
T_c=600 K T_m=300 K Temperature dependent	Si_3N_4	11.799	28.033	42.677	51.657	64.394
	0.5	8.264	19.639	29.894	36.164	45.073
	1.0	7.286	17.233	26.055	31.343	38.713
	2.0	6.571	15.580	23.673	28.585	35.579
	SUS304	5.086	12.140	18.521	22.323	27.851
T_c=600 K T_m=300 K Temperature independent	Si_3N_4	12.185	28.890	43.950	53.198	66.293
	0.5	8.445	20.049	30.509	36.910	45.996
	1.0	7.417	17.558	26.680	32.060	39.862
	2.0	6.656	15.773	23.959	28.927	35.999
	SUS304	5.309	12.644	19.265	23.245	28.981

Additionally, the variation of fundamental frequencies with change in temperature of the upper side is also shown in Tables 7 and 8.

Variations of the fundamental frequencies versus foundation parameters of plates lying on Winkler and Pasternak elastic foundation are respectively shown in Figure 3(a), (b), and Figure 3(c), (d) for different power-law index k and modes 1 and 3. All the plates are subjected to a nonlinear thermal rise of 400 K. It is noted that by increasing the power-law index, the fundamental frequencies decrease whatever the type of foundation. This decrease is because an increase in the power-law index decreases the elasticity modulus. In other words, the plate becomes softer as the metal's volume fraction increases, thus decreasing the frequencies' values.

The variation of Winkler foundation stiffness slightly affects the fundamental frequencies only in the first mode, see Figure 3(a). Otherwise, its influence is neglected (Figure 3(b)). However, the results presented in Figure 3(c) and (d) show that the fundamental frequencies of the plate increase with the increase of Pasternak foundation's stiffness, whatever k, and the mode vibration. Because when the parameter k_p increases, it increases the bending stiffness of the plate and therefore entrains the increase of the natural frequency.

Variations of the fundamental frequencies of FG plates subjected to nonlinear temperature difference and resting on Winkler/Pasternak elastic foundation are respectively shown in Figure 4(a) and (b) using a power-law index k=1. The maximum values of fundamental frequencies are obtained for

Table 7. 3D fundamental frequencies $\bar{\omega}$ of FG square plates lying on Winkler/Pasternak foundations with a/b=1 and a=8 h.

T	k_w	k_p	k	Modes				
				(1, 1)	(1, 2)	(2, 2)	(1, 3)	(2, 3)
T_c=400 K T_m=300 K	0	0	Si_3N_4	12.204	28.757	43.655	52.843	65.786
			0.5	8.510	20.049	30.425	36.813	45.814
			1.0	7.490	17.555	26.454	31.810	39.200
			2.0	6.746	15.844	23.986	28.974	35.995
			SUS304	5.395	12.709	19.270	23.275	28.939
	100	0	Si_3N_4	13.290	29.216	43.950	53.083	65.976
			0.5	9.361	20.410	30.656	37.001	45.963
			1.0	8.278	17.891	26.671	31.989	39.342
			2.0	7.483	16.159	24.189	29.140	36.126
			SUS304	6.092	13.008	19.463	23.433	29.064
	0	100	Si_3N_4	26.363	46.247	62.808	72.820	86.782
			0.5	19.297	33.482	45.187	52.234	62.046
			1.0	17.348	29.918	40.140	46.193	54.487
			2.0	15.890	27.344	36.708	42.312	50.097
			SUS304	13.550	22.938	30.540	35.002	41.291
	100	100	Si_3N_4	26.883	46.533	63.013	72.994	86.926
			0.5	19.686	33.698	45.343	52.367	62.156
			1.0	17.702	30.115	40.283	46.316	54.589
			2.0	16.216	27.527	36.840	42.426	50.192
			SUS304	13.962	23.415	31.126	35.725	42.121
T_c=600 K T_m=300 K	0	0	Si_3N_4	11.799	28.033	42.677	51.657	64.394
			0.5	8.264	19.639	29.894	36.164	45.073
			1.0	7.286	17.233	26.055	31.343	38.713
			2.0	6.571	15.580	23.673	28.585	35.579
			SUS304	5.086	12.140	18.521	22.323	27.851
	100	0	Si_3N_4	12.919	28.503	42.978	51.903	64.587
			0.5	9.138	20.007	30.130	36.356	45.224
			1.0	8.094	17.575	26.276	31.524	38.857
			2.0	7.326	15.900	23.879	28.754	35.712
			SUS304	5.819	12.452	18.721	22.488	27.981
	0	100	Si_3N_4	26.178	45.800	62.132	71.964	85.732
			0.5	19.190	33.239	44.835	51.784	61.507
			1.0	17.262	29.732	39.883	45.876	54.140
			2.0	15.817	27.194	36.508	42.053	49.807
			SUS304	13.673	23.251	31.006	35.621	42.034
	100	100	Si_3N_4	26.701	46.089	62.340	72.140	85.877
			0.5	19.582	33.458	44.992	51.918	61.617
			1.0	17.617	29.931	40.027	45.999	54.243
			2.0	16.145	27.379	36.642	42.167	49.901
			SUS304	13.841	23.105	30.662	35.108	41.379

(k_w=k_p=100); this is due mainly to the inclusion of the shear layer, which stabilizes the lateral movement of the plate. However, the minimum ones are reached for plates without shear layer (k_p=0). The fundamental frequencies decrease with the increase of the environment temperature's change.

The reason is that increasing the temperature results in a decrease of the material rigidity while the system's mass remains constant.

Figure 5 gives the fundamental frequencies of various plates versus Kerr foundation's parameters (k_l, k_u, and k_s) under a nonlinear temperature change of 400 K using a different power-law index. Whatever the power-law index, all the curves exhibit almost the same evolution. The fundamental frequencies fall rapidly when the parameter of the lower elastic layer is small (k_l<30), while they slowly change when k_l>30 (Figure 5(a)). However, they rise rapidly when the parameter of the upper elastic layer is small (k_u<30), while they slowly change when k_u>30 (see Figure 5(b)). More importantly, Figure 5(c) gives the fundamental natural frequency versus shear layer parameter for different FG plates. Notably, the fundamental frequencies increase considerably as the shear parameter (k_s) increases.

Table 8. 3D fundamental frequencies $\bar{\omega}$ of FG square plates lying on Kerr foundation with a/b=1, a=8 h and k_l=100.

T	k_u	k_s	k	Modes (1, 1)	(1, 2)	(2, 2)	(1, 3)	(2, 3)
			Si_3N_4	12.759	28.987	43.803	52.963	65.881
			0.5	8.946	20.230	30.541	36.907	45.888
	100	0	1.0	7.894	17.726	26.562	31.912	39.296
			2.0	7.124	16.002	24.087	29.057	36.060
			SUS304	5.754	12.859	19.367	23.354	29.002
			Si_3N_4	12.204	28.757	43.655	52.843	65.786
			0.5	8.510	20.049	30.425	36.813	45.814
T_c=400 K T_m=300 K	0	100	1.0	7.490	17.557	26.454	31.823	39.225
			2.0	6.746	15.844	23.986	28.974	35.995
			SUS304	5.395	12.709	19.270	23.275	28.939
			Si_3N_4	20.878	38.682	54.206	63.720	77.084
			0.5	15.168	27.730	38.614	45.266	54.604
	100	100	1.0	13.594	24.654	34.081	39.744	47.546
			2.0	12.421	22.462	31.088	36.331	43.677
			SUS304	10.586	18.840	25.887	30.150	36.136
			Si_3N_4	12.372	28.269	42.828	51.780	64.491
			0.5	8.712	19.824	30.012	36.260	45.148
	100	0	1.0	7.701	17.404	26.165	31.430	38.779
			2.0	6.959	15.741	23.776	28.670	35.646
			SUS304	5.465	12.297	18.622	22.406	27.916
			Si_3N_4	11.799	28.033	42.677	51.657	64.394
			0.5	8.264	19.639	29.894	36.164	45.073
T_c=600 K T_m=300 K	0	100	1.0	7.286	17.233	26.055	31.339	38.706
			2.0	6.571	15.580	23.673	28.585	35.579
			SUS304	5.086	12.140	18.521	22.323	27.851
			Si_3N_4	20.644	38.146	53.421	62.740	75.899
			0.5	15.032	27.436	38.200	44.743	53.986
	100	100	1.0	13.483	24.425	33.775	39.362	47.123
			2.0	12.328	22.278	30.849	36.025	43.339
			SUS304	10.429	18.457	25.330	29.419	35.270

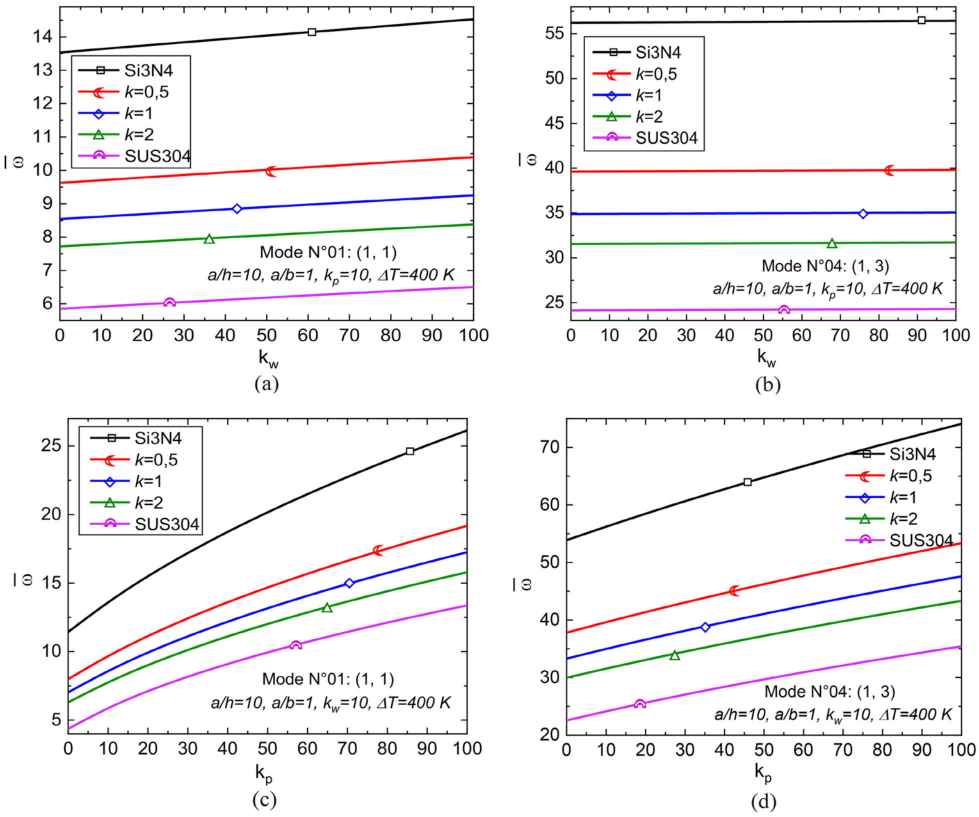

Figure 3. Variation of $\bar{\omega}$ of square plates versus the elastic foundation parameters (k_w and k_p) under nonlinear temperature gradient (ΔT=400 K) (a) effect of k_w in first mode, (b) effect of k_w in fourth mode, (c) effect of k_p in first mode, and (d) effect of k_p in fourth mode.

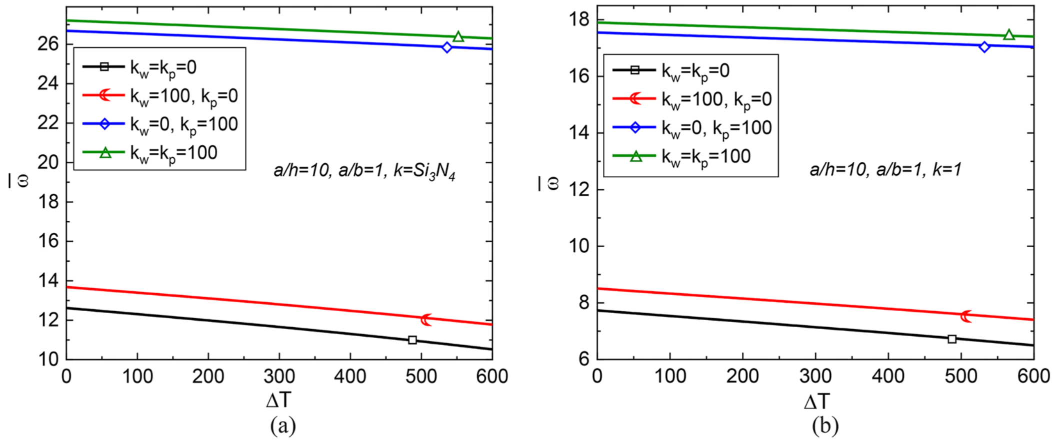

Figure 4. 3D fundamental frequencies $\bar{\omega}$ depending on the nonlinear temperature change ΔT of the square plates lying on different elastic foundations: (a) Homogenous plate (k=0) and (b) FG plate (k=1).

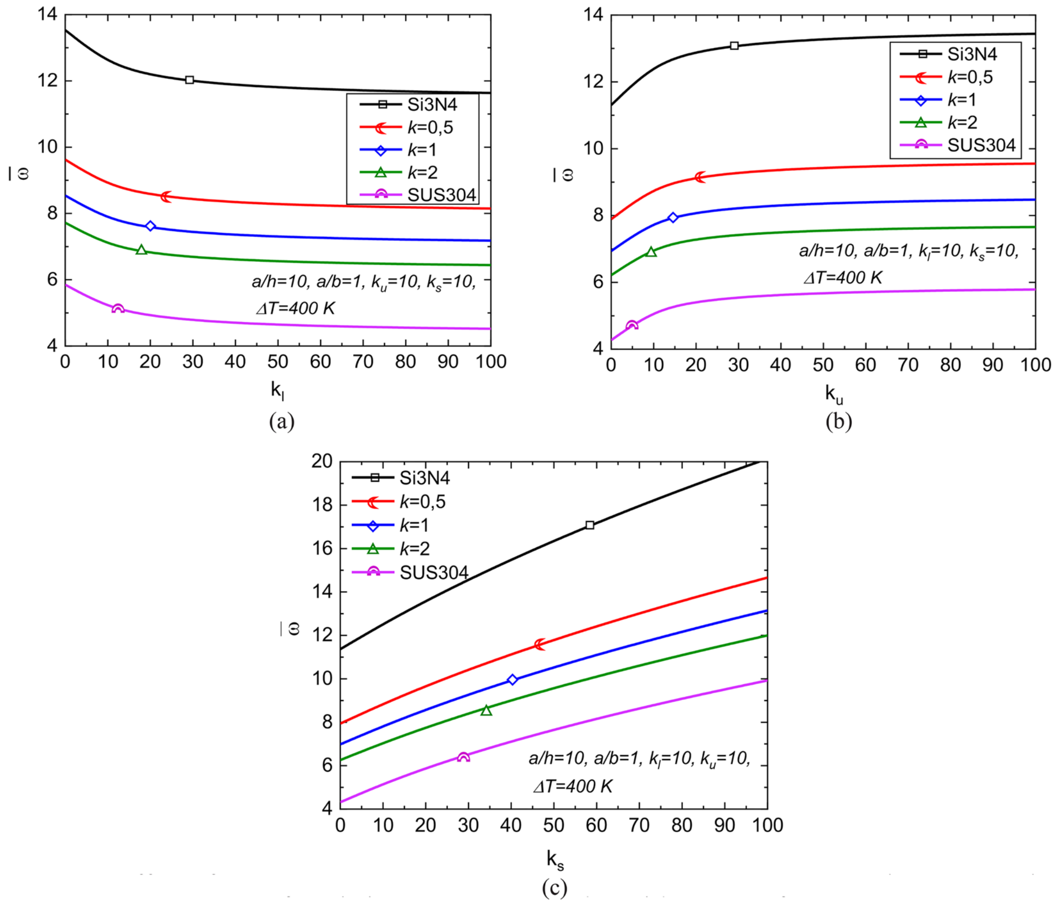

Figure 5. Effect of Kerr foundation parameters (k_l, k_u and k_s) on $\bar{\omega}$ of square plates exposed to nonlinear temperature change (ΔT=400 K).

The effect of parameters (k_l, k_u, k_s, ΔT) on the fundamental frequencies of square plates are also studied, (see Figure 6).

Based on the variation of slope of fundamental frequencies, it is observed that increasing (k_l, k_u, k_s) has an insignificant influence on the effect of the ΔT on the frequency of homogenous as well as FG plates. In other words, whatever the Kerr foundation's parameters, the fundamental frequencies decrease slightly as ΔT increases. However, the lower spring, upper spring, and shear layer parameters have rising effects on the fundamental frequencies of FG plates.

Figure 7(a), (b) and Figure 7(c), (d) display a 3D analysis of fundamental frequency versus slenderness ratio *a/h* for homogenous plate (k=0) and FG square plates lying on two types of foundation and exposed to various nonlinear temperature changes: 0, 100, 200, 300, and 400 K, respectively. As highlighted in Figure 7, the first natural frequencies are almost constant at ΔT=0, whatever the foundation type. But, for high-temperature changes, the frequencies fall with growing *a/h* until it becomes zero. Therefore, the critical slenderness ratio for plates lying on the Winkler-Pasternak foundation is higher than that on the Kerr foundation.

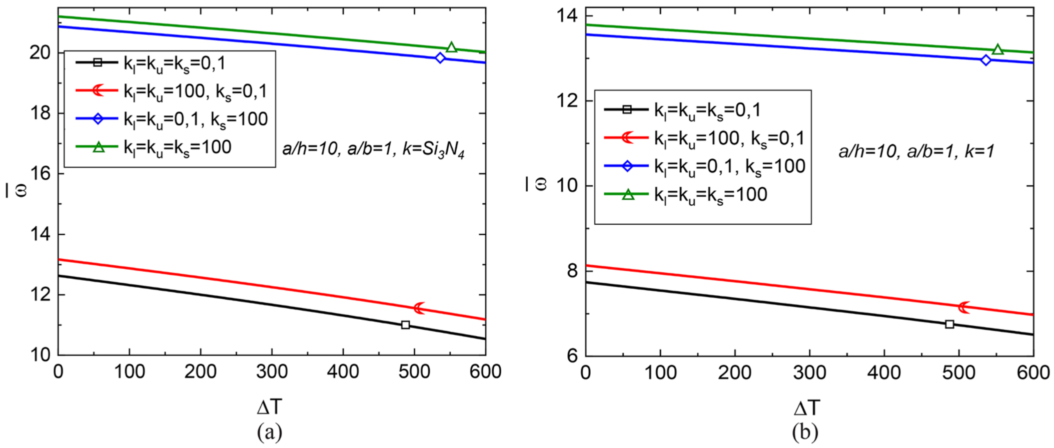

Figure 6. 3D $\bar{\omega}$ depending on the nonlinear temperature change ΔT of the square plates lying on different Kerr foundations: (a) Homogenous plate (k=0) and (b) FG plate (k=1).

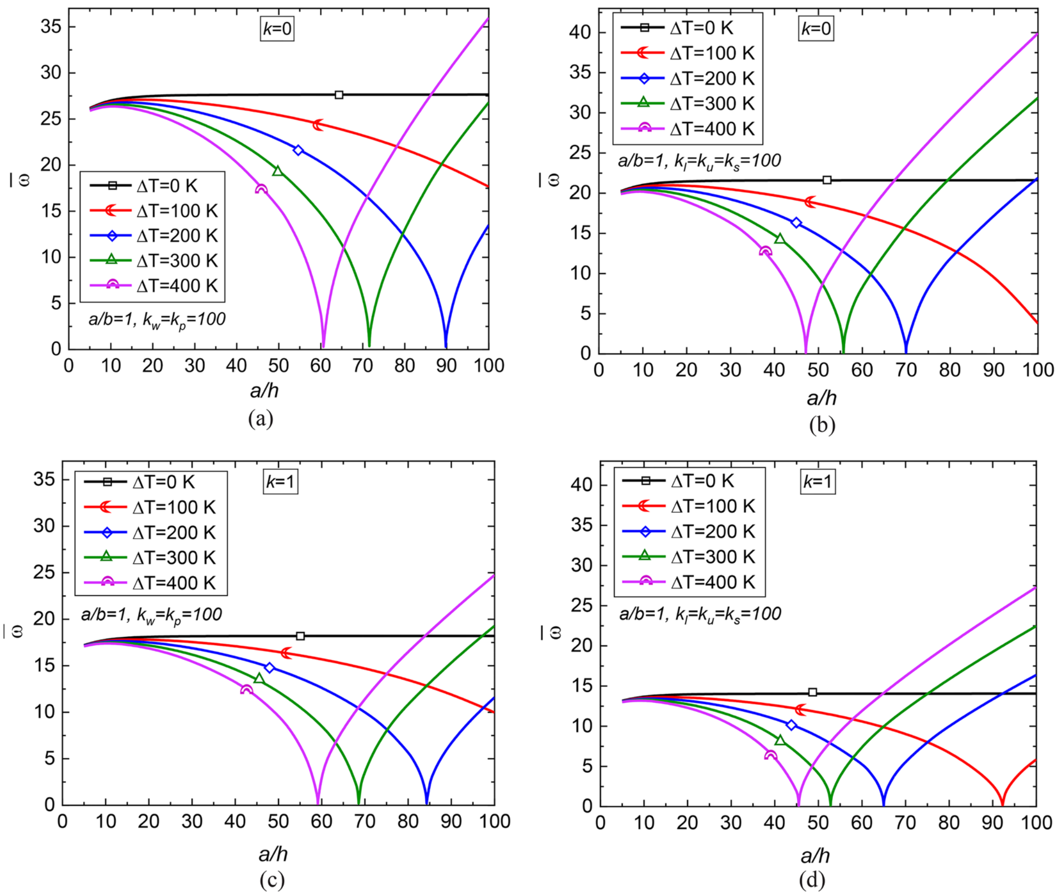

Figure 7. 3D fundamental frequencies $\bar{\omega}$ of square plates lying on two types of foundations and exposed to various nonlinear temperature changes (ΔT) versus the side-to-thickness ratio (a-b) Homogenous plate (k=0), and (c-d) FG plate (k=1).

Figure 8 (a), (b) and Figure 8 (c), (d) show the influence of the aspect ratio b/a on the fundamental frequencies of the homogenous plate (k=0) and FG square plates lying on two types of foundation and exposed to various nonlinear temperature changes: 0, 100, 200, 300, and 400 K, respectively. Importantly, it is found that increasing b/a reduces the frequencies of the structures significantly. More importantly, the fundamental frequencies drop rapidly when the aspect ratio is small (b/a <6) while they become constant b/a>6 (Figure 8(a)). Furthermore, the frequencies are decreased with increasing the temperature change ΔT, and this effect becomes more remarkable with increasing the aspect ratio b/a.

6. Conclusions

In this study, the new four-unknown shear deformation theory is used to analyze the 3D free thermal vibration of Functionally Graded Martial (FGM) plates for the first time. The governing equations are established based on Hamilton's principle. Validation studies have been performed to confirm the relevance of the current theory formulation. The obtained results are very similar to those published by various researchers.

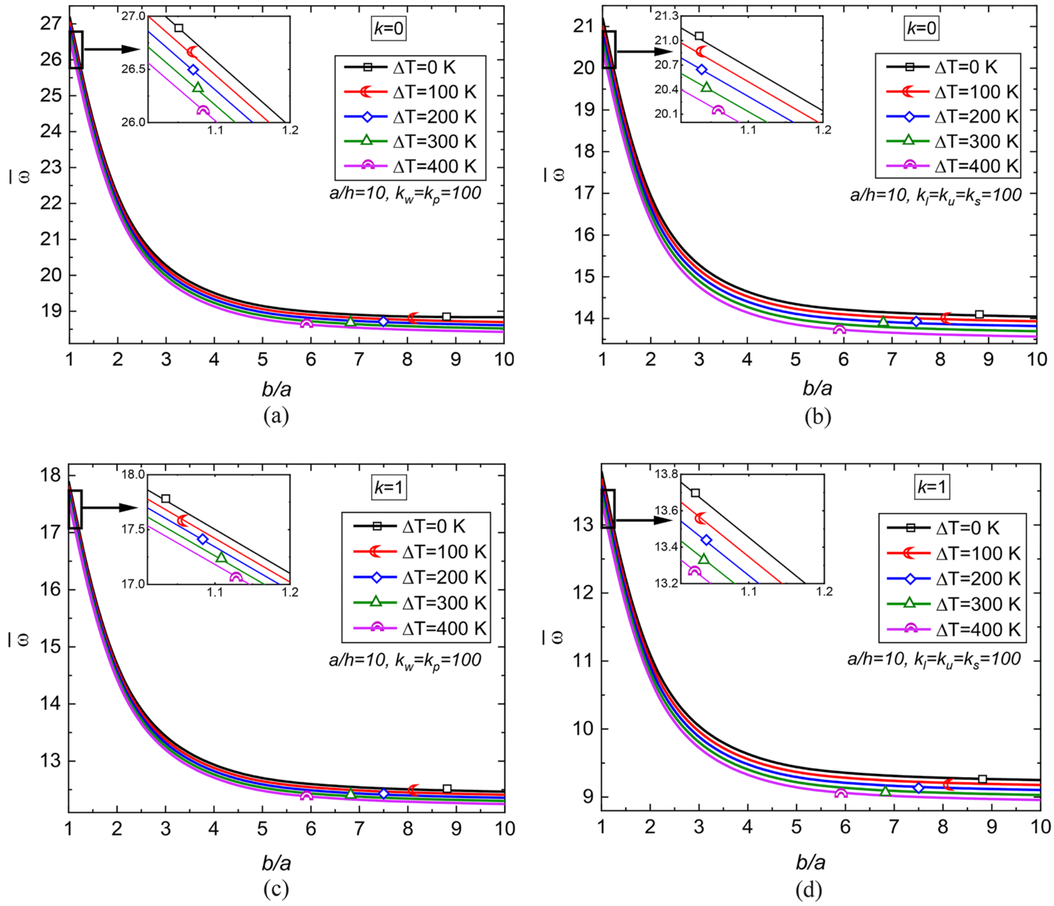

Figure 8: 3D fundamental frequencies $\bar{\omega}$ of square plates lying on two types of foundations and exposed to various nonlinear temperature changes (*ΔT*) versus the plate aspect ratio (a-b) Homogenous plate (*k*=0) and (c-d) FG plate (*k*=1).

- The increase in elastic foundation parameters would enhance the free-vibrational response of homogenous and FG plates in the same manner. However, this increase has an insignificant influence on the effect of the temperature change (*ΔT*) on the fundamental frequencies of these structures,
- The increase in the temperature change (*ΔT*) softens the FG plate and reduces the natural frequency. This reduction is related to the compressive stress caused by the thermal gradients,
- The effect of the plate's configuration is more significant when the nonlinear temperature difference (*ΔT*) is at high levels,
- Even at high temperatures, the Pasternak/Kerr foundation models are suitable for performing free-vibrational analysis of Functionally Graded (FG) plates using large values of shear layer stiffness,
- Pasternak foundation model is better suited for the free-vibrational response of FG plates than the Kerr foundation model. For large values of upper spring modulus, the Kerr model tends to that of Pasternak.

Declaration of competing interest

The authors declare that they have no known competing financial interests or personal relationships that could have appeared to influence the work reported in this paper.

Funding

This research did not receive any specific grant from funding agencies in the public, commercial, or not-for-profit sectors.

Conflicts of interest

The authors declare that they have no known competing financial interests or personal relationships that could have appeared to influence the work reported in this paper.

Authors contribution statement

Belgacem Mamen:
Conceptualization; Data curation; Formal analysis; Writing–review and editing.
Abdelhakim Bouhadra:
Investigation; Methodology; Software; Supervision; Writing review and editing.
Fouad Bourada : Software; Supervision.
Mohamed Bourada : Supervision.
Abdelouahed Tounsi: Methodology; Supervision.
Muzamal Hussain: Supervision.

References

1. Sayyad, A.S. and Ghugal, Y.M. "Modeling and analysis of functionally graded sandwich beams: A review", *Mechanics of Advanced Materials and*

Structures, **26**(21), pp. 1776-1795 (2019). https://doi.org/10.1080/15376494.2018.1447178.

2. Thai, H.T., Nguyen, T.K., Vo, T.P., et al. "Analysis of functionally graded sandwich plates using a new first-order shear deformation theory", *European Journal of Mechanics-A/Solids*, **45**, pp. 211-225 (2014). https://doi.org/10.1016/j.euromechsol.2013.12.008.

3. Huang, X.L. and Shen, H.S. "Nonlinear vibration and dynamic response of functionally graded plates in thermal environments", *International Journal of Solids and Structures*, **41**(9-10), pp. 2403-2427 (2004). https://doi.org/10.1016/j.ijsolstr.2003.11.012.

4. Lei, Z.X., Zhang, L.W., and Liew, K.M. "Buckling analysis of CNT reinforced functionally graded laminated composite plates", *Composite Structures*, **152**, pp. 62-73 (2016). https://doi.org/10.1016/j.compstruct.2016.05.047.

5. Sayyad, A.S., and Ghugal, Y.M. "A unified shear deformation theory for the bending of isotropic, functionally graded, laminated and sandwich beams and plates", *International Journal of Applied Mechanics*, **9**(01), 1750007 (2017). https://doi.org/10.1142/S1758825117500077.

6. Parida, S. and Mohanty, S.C. "Free vibration analysis of rotating functionally graded material plate under nonlinear thermal environment using higher order shear deformation theory", *Proceedings of the Institution of Mechanical Engineers, Part C: Journal of Mechanical Engineering Science*, **233**(6), pp. 2056-2073 (2018). https://doi.org/10.1177/0954406218777535.

7. Van Do, V.N. and Lee, C.H. "Quasi-3D isogeometric buckling analysis method for advanced composite plates in thermal environments", *Aerospace Science and Technology*, **92**, pp. 34-54 (2019). https://doi.org/10.1016/j.ast.2019.05.056.

8. Li, S.R. and Ma, H.K. "Analysis of free vibration of functionally graded material micro-plates with thermoelastic damping", *Archive of Applied Mechanics*, **90**(6), pp. 1285-1304 (2020). https://doi.org/10.1007/s00419-020-01664-9.

9. Mehditabar, A., Rahimi, G.H., and Vahdat, S.E. "Integrity assessment of functionally graded pipe produced by centrifugal casting subjected to internal pressure: experimental investigation", *Archive of Applied Mechanics*, **90**(8), pp. 1723-1736 (2020). https://doi.org/10.1007/s00419-020-01692-5.

10. Guerroudj, H.Z., Yeghnem, R., Kaci, A., et al. "Eigenfrequencies of advanced composite plates using an efficient hybrid quasi-3D shear deformation theory", *Smart Structures and Systems*, **22**(1), pp. 121-132 (2018). https://doi.org/10.12989/sss.2018.22.1.121.

11. Mahmoudi, A., Benyoucef, S., Tounsi, A., et al. "On the effect of the micromechanical models on the free vibration of rectangular FGM plate resting on elastic foundation", *Earthquakes and Structures*, **14**(2), p. 117 (2018). https://doi.org/10.12989/eas.2018.14.2.117.

12. Zenkour, A.M. and Radwan, A.F. "Hygrothermo-mechanical buckling of FGM plates resting on elastic foundations using a quasi-3D model", *International Journal for Computational Methods in Engineering Science and Mechanics*, **20**(2), pp. 85-98 (2019). https://doi.org/10.1080/15502287.2019.1568618.

13. Woodward, B. and Kashtalyan, M. "Three-dimensional elasticity analysis of sandwich panels with functionally graded transversely isotropic core", *Archive of Applied Mechanics*, **89**, pp. 2463-2484 (2019). https://doi.org/10.1007/s00419-019-01589-y.

14. Hieu, P.T., and Van Tung, H. "Thermal and thermomechanical buckling of shear deformable FG-CNTRC cylindrical shells and toroidal shell segments with tangentially restrained edges", *Archive of Applied Mechanics*, **90**(7), pp. 1529-1546 (2020). https://doi.org/10.1007/s00419-020-01682-7.

15. Ye, R., Zhao, N., Yang, D., et al. "Bending and free vibration analysis of sandwich plates with functionally graded soft core, using the new refined higher-order analysis model", *Journal of Sandwich Structures & Materials*, **23**(2), pp. 680-710 (2021). https://doi.org/10.1177/1099636220909763.

16. Shariyat, M. "A generalized global–local high-order theory for bending and vibration analyses of sandwich plates subjected to thermo-mechanical loads", *International Journal of Mechanical Sciences*, **52**(3), pp. 495-514 (2010). https://doi.org/10.1016/j.ijmecsci.2009.11.010.

17. Malekzadeh, P. and Monajjemzadeh, S.M. "Dynamic response of functionally graded plates in thermal environment under moving load", *Composites Part B: Engineering*, **45**(1), pp. 1521-1533 (2013). https://doi.org/10.1016/j.compositesb.2012.09.022.

18. Attia, A., Tounsi, A., Bedia, E.A., et al. "Free vibration analysis of functionally graded plates with temperature-dependent properties using various four variable refined plate theories", *Steel Compos. Struct*, **18**(1), pp. 187-212 (2015). http://dx.doi.org/10.12989/scs.2015.18.1.187.

19. Zaoui, F.Z., Ouinas, D., Tounsi, A., et al. "Fundamental frequency analysis of functionally graded plates with temperature-dependent properties based on improved exponential-trigonometric two-dimensional higher shear deformation theory", *Archive of Applied Mechanics*, **91**(3), pp. 859-881 (2021).

https://doi.org/10.1007/s00419-020-01793-1.

20. Arshid, E., Arshid, H., Amir, S., et al. "Free vibration and buckling analyses of FG porous sandwich curved microbeams in thermal environment under magnetic field based on modified couple stress theory", *Archives of Civil and Mechanical Engineering*, **21**, pp. 1-23 (2021). https://doi.org/10.1007/s43452-020-00150-x.

21. Li, C., Shen, H.S., and Yang, J. "Nonlinear vibration behavior of FG sandwich beams with auxetic porous copper core in thermal environments", *International Journal of Structural Stability and Dynamics*, **23**(13), 2350144 (2023). https://doi.org/10.1142/S0219455423501444.

22. Singha, T.D., Bandyopadhyay, T., and Karmakar, A. "A numerical solution for thermal free vibration analysis of rotating pre-twisted FG-GRC cylindrical shell panel", *Mechanics of Advanced Materials and Structures*, **30**(15), pp. 3013-3031 (2023). https://doi.org/10.1080/15376494.2022.2067924.

23. Abouelregal, A.E., Mohammad-Sedighi, H., Faghidian, S.A., et al. "Temperature-dependent physical characteristics of the rotating nonlocal nanobeams subject to a varying heat source and a dynamic load", *Facta Universitatis, Series: Mechanical Engineering*, **19**(4), pp. 633-656 (2021). https://doi.org/10.22190/FUME201222024A.

24. Nasr, M.E., Abouelregal, A.E., Soleiman, A., et al. "Thermoelastic Vibrations of Nonlocal Nanobeams Resting on a Pasternak Foundation via DPL Model", *Journal of Applied and Computational Mechanics*, **7**(1), pp. 34-44 (2021). https://doi.org/10.22055/jacm.2020.34228.2362.

25. Malekzadeh, P., Shahpari, S.A. and Ziaee, H.R. "Three-dimensional free vibration of thick functionally graded annular plates in thermal environment", *Journal of Sound and Vibration*, **329**(4), pp. 425-442 (2010). https://doi.org/10.1016/j.jsv.2009.09.025.

26. Malekzadeh, P., and Safaeian Hamzehkolaei, N. "A 3D discrete layer-differential quadrature free vibration of multi-layered FG annular plates in thermal environment", *Mechanics of Advanced Materials and Structures*, **20**(4), pp. 316-330 (2013). https://doi.org/10.1080/15376494.2011.627637.

27. Tu, T.M., Quoc, T.H., and Van Long, N. "Vibration analysis of functionally graded plates using the eight-unknown higher order shear deformation theory in thermal environments", *Aerospace Science and Technology*, **84**, pp. 698-711 (2019). https://doi.org/10.1016/j.ast.2018.11.010.

28. Zaoui, F.Z., Tounsi, A., and Ouinas, D. "Free vibration of functionally graded plates resting on elastic foundations based on quasi-3D hybrid-type higher order shear deformation theory", *Smart Structures and Systems*, **20**(4), pp. 509-524 (2017). https://doi.org/10.12989/sss.2017.20.4.509.

29. Zhou, L. "A novel similitude method for predicting natural frequency of FG porous plates under thermal environment", *Mechanics of Advanced Materials and Structures*, **29**(27), pp. 6786-6802 (2022). https://doi.org/10.1080/15376494.2021.1985197.

30. Mamen, B., Bouhadra, A., Bourada, F., et al. "Combined effect of thickness stretching and temperature-dependent material properties on dynamic behavior of imperfect FG beams using three variable quasi-3D model", *Journal of Vibration Engineering & Technologies*, **11**(5), pp. 1-23 (2022). https://doi.org/10.1007/s42417-022-00704-8.

31. Touloukian, Y.S. "Thermophysical properties of high temperature solid materials", Volume 4. Oxides and their solutions and mixtures. Part I. Simple oxygen compounds and their mixtures. *Defense Technical Information Center*, (1966). DTIC AD0649951.

32. Salari, E., Ashoori, A.R., Vanini, S.S., et al. "Nonlinear dynamic buckling and vibration of thermally post-buckled temperature-dependent FG porous nanobeams based on the nonlocal theory", *Physica Scripta*, **97**(8), 085216 (2022). https://doi.org/10.1088/1402-4896/ac8187.

33. Javaheri, R. and Eslami, M.R. "Thermal buckling of functionally graded plates based on higher order theory", *Journal of Thermal Stresses*, **25**(7), pp. 603-625 (2002). https://doi.org/10.1080/01495730290074333.

34. Shahrjerdi, A., Mustapha, F., Bayat, M., et al. "Free vibration analysis of solar functionally graded plates with temperature-dependent material properties using second order shear deformation theory", *Journal of Mechanical Science and Technology*, **25**(9), pp. 2195-2209 (2011). https://doi.org/10.1007/s12206-011-0610-x.

35. Ebrahimi, F., and Barati, M.R. "Temperature distribution effects on buckling behavior of smart heterogeneous nanosize plates based on nonlocal four-variable refined plate theory", *International Journal of Smart and Nano Materials*, **7**(3), pp. 119-143 (2016). https://doi.org/10.1080/19475411.2016.1223203

36. Bouhadra, A., Menasria, A., and Rachedi, M.A. "Boundary conditions effect for buckling analysis of porous functionally graded nanobeams", *Advances in Nano Research*, **10**(4), p. 313 (2021). https://doi.org/10.12989/anr.2021.10.4.313.

37. Esmaeilzadeh, M. and Kadkhodayan, M. "Dynamic analysis of stiffened bi-directional functionally graded plates with porosities under a moving load by dynamic relaxation method with kinetic damping", *Aerospace Science and Technology*, **93**, 105333 (2019). https://doi.org/10.1016/j.ast.2019.105333.

38. Li, S.R., Su, H.D. and Cheng, C.J. "Free vibration of functionally graded material beams with surface-bonded piezoelectric layers in thermal environment", *Applied Mathematics and Mechanics*, **30**(8), pp. 969-982 (2009). https://doi.org/10.1007/s10483-009-0803-7.

39. Li, M., Soares, C.G., and Yan, R. "Free vibration analysis of FGM plates on Winkler/Pasternak/Kerr foundation by using a simple quasi-3D HSDT", *Composite Structures*, **264**, 113643 (2021). https://doi.org/10.1016/j.compstruct.2021.113643.

40. Reddy, J.N. and Chin, C.D. "Thermomechanical analysis of functionally graded cylinders and plates". *Journal of Thermal Stresses*, **21**(6), pp. 593-626 (1998). https://doi.org/10.1080/01495739808956165.

Appendix A

$$\begin{Bmatrix} N_x \\ N_y \\ N_{xy} \\ M_x^b \\ M_y^b \\ M_{xy}^b \\ M_x^s \\ M_y^s \\ M_{xy}^s \\ N_z \\ Q_{yz}^s \\ Q_{xz}^s \\ S_{yz}^s \\ S_{xz}^s \end{Bmatrix} = \begin{bmatrix} A_{11} & A_{12} & 0 & B_{11} & B_{12} & 0 & 0 & B_{12}^s k_2 B' & B_{11}^s k_1 A' & L & 0 & 0 & 0 & 0 \\ A_{12} & A_{22} & 0 & B_{12} & B_{22} & 0 & 0 & B_{22}^s k_2 B' & B_{12}^s k_1 A' & L & 0 & 0 & 0 & 0 \\ 0 & 0 & A_{66} & 0 & 0 & B_{66} & B_{66}^s(k_1 A' + k_2 B') & 0 & 0 & 0 & 0 & 0 & 0 & 0 \\ B_{11} & B_{12} & 0 & D_{11} & D_{12} & 0 & 0 & D_{12}^s k_2 B' & D_{11}^s k_1 A' & L_a & 0 & 0 & 0 & 0 \\ B_{12} & B_{22} & 0 & D_{12} & D_{22} & 0 & 0 & D_{22}^s k_2 B' & D_{12}^s k_1 A' & L_a & 0 & 0 & 0 & 0 \\ 0 & 0 & B_{66} & 0 & 0 & D_{66} & D_{66}^s(k_1 A' + k_2 B') & 0 & 0 & 0 & 0 & 0 & 0 & 0 \\ B_{11}^s & B_{12}^s & 0 & D_{11}^s & D_{12}^s & 0 & 0 & H_{12}^s k_2 B' & H_{11}^s k_1 A' & R & 0 & 0 & 0 & 0 \\ B_{12}^s & B_{22}^s & 0 & D_{12}^s & D_{22}^s & 0 & 0 & H_{22}^s k_2 B' & H_{12}^s k_1 A' & R & 0 & 0 & 0 & 0 \\ 0 & 0 & B_{66}^s & 0 & 0 & D_{66}^s & 0 & 0 & H_{66}^s(k_1 A' + k_2 B') & 0 & 0 & 0 & 0 & 0 \\ L & L & 0 & L_a & L_a & 0 & 0 & k_2 B' R & k_1 A' R & R_a & 0 & 0 & 0 & 0 \\ 0 & 0 & 0 & 0 & 0 & 0 & 0 & 0 & 0 & 0 & F_{44}^s (k_2 B')^2 + X_{44}^s & 0 & 0 & 0 \\ 0 & 0 & 0 & 0 & 0 & 0 & 0 & 0 & 0 & 0 & 0 & F_{55}^s (k_1 A')^2 + X_{55}^s & 0 & 0 \\ 0 & 0 & 0 & 0 & 0 & 0 & 0 & 0 & 0 & 0 & X_{44}^s k_2 B' + A_{44}^s & 0 & 0 & 0 \\ 0 & 0 & 0 & 0 & 0 & 0 & 0 & 0 & 0 & 0 & 0 & X_{55}^s k_1 A' + A_{55}^s & 0 & 0 \end{bmatrix} \begin{Bmatrix} \frac{\partial u_0}{\partial x} \\ \frac{\partial v_0}{\partial y} \\ \frac{\partial u_0}{\partial y} + \frac{\partial v_0}{\partial x} \\ -\frac{\partial^2 w_0}{\partial x^2} \\ -\frac{\partial^2 w_0}{\partial y^2} \\ -2\frac{\partial^2 w_0}{\partial x \partial y} \\ \frac{\partial^2 \theta}{\partial x \partial y} \\ \frac{\partial^2 \theta}{\partial y^2} \\ \frac{\partial^2 \theta}{\partial x^2} \\ \theta \\ \frac{\partial \theta}{\partial y} \\ \frac{\partial \theta}{\partial x} \\ 0 \\ 0 \end{Bmatrix}$$

Appendix B

$$d_{11} = [-A_{11}\lambda^2 - A_{66}\beta^2 - I_0 {\omega_n}^2],$$

$$d_{12} = d_{21} = [-(A_{11} + A_{66})\lambda\beta],$$

$$d_{13} = d_{31} = [B_{11}\lambda^3 + (B_{12} + 2B_{66})\lambda\beta^2 + I_1 {\omega_n}^2 \lambda],$$

$$d_{14} = d_{41} = \left[-k_1 A' J_1 \lambda {\omega_n}^2 - \left(B_{12}^s k_2 B' + B_{66}^s (k_1 A' + k_2 B')\right)\lambda\beta^2 - B_{11}^s k_1 A' \lambda^3 + L\lambda\right],$$

$$d_{22} = [-A_{22}\beta^2 - A_{66}\lambda^2 - I_0 {\omega_n}^2],$$

$$d_{23} = d_{32} = [I_1 {\omega_n}^2 \beta + B_{22}\beta^3 + (B_{12} + 2B_{66})\lambda^2\beta],$$

$$d_{24} = d_{42} = \left[-k_2 B' J_1 \beta {\omega_n}^2 - \left(B_{12}^s k_1 A' + B_{66}^s (k_1 A' + k_2 B')\right)\beta\lambda^2 - B_{22}^s k_2 B' \beta^3 + L\beta\right],$$

$$d_{33} = \begin{bmatrix} -{\omega_n}^2\left(I_0 + I_2(\lambda^2 + \beta^2)\right) - 2(D_{12} + 2D_{66})\lambda^2\beta^2 - D_{22}\beta^4 - D_{11}\lambda^4 \\ -K_w - K_p(\lambda^2 + \beta^2) - \left(\dfrac{K_l K_u}{K_l + K_u}\right) - \left(\dfrac{K_s K_u}{K_l + K_u}\right)(\lambda^2 + \beta^2) + N^T(\lambda^2 + \beta^2) - 2{N_{xy}}^T(\lambda\beta) \end{bmatrix},$$

$$d_{34} = d_{43} = \begin{bmatrix} -{\omega_n}^2\left(-J_2(k_1 A' \lambda^2 + k_2 B' \beta^2) + J_0\right) + D_{11}^s k_1 A' \lambda^4 + (D_{12}^s + 2D_{66}^s)(k_1 A' + k_2 B')\lambda^2\beta^2 \\ +D_{22}^s k_2 B' \beta^4 - L_a(\lambda^2 + \beta^2) + g(0) N^T(\lambda^2 + \beta^2) - 2{N_{xy}}^T g(0)(\lambda\beta) \end{bmatrix},$$

$$d_{44} = \begin{bmatrix} -{\omega_n}^2\left(K_2\left((k_1 A')^2\lambda^2 + (k_2 B')^2\beta^2\right) + K_0\right) - (k_1 A')^2 H_{11}^s \lambda^4 - (k_2 B')^2 H_{22}^s \beta^4 \\ -\left(2H_{12}^s k_1 A' k_2 B' + H_{66}^s (k_1 A' + k_2 B')^2\right)\lambda^2\beta^2 \\ +\left(-F_{55}^s (k_1 A')^2 + 2k_1 A' R - 2k_1 A' X_{55}^s - A_{55}^s\right)\lambda^2 \\ +\left(-F_{44}^s (k_2 B')^2 + 2k_2 B' R - 2k_2 B' X_{44}^s - A_{44}^s\right)\beta^2 - R_a \\ +N^T g(0)^2(\lambda^2 + \beta^2) - 2{N_{xy}}^T g(0)^2(\lambda\beta) \end{bmatrix}$$

Biographies

Belgacem Mamen holds a MSc degree (2010) in Modeling and Experimentation in Solid Mechanics from Joseph Fourier University and INPG Institute, Grenoble (FRANCE). He received his PhD degree (2013) in Engineering Sciences (Mechanics, Mechanical Engineering, Civil Engineering) from Franche-Comté University, Besançon (FRANCE). He is an Associate Professor in Structural Engineering at the Department of Civil Engineering at Abbes Laghrour University of Khenchela (ALGERIA). He has supervised three PhD theses and more than ten MSc students. His interests include experimental research, composite material, thermomechanical modeling, numerical analysis, and programming, especially Maple and ABAQUS.

Abdelhakim Bouhadra holds a PhD degree (2015) in Civil Engineering from Djillali Liabes University of Sidi Bel Abbes (ALGERIA). He is an Associate Professor in Structural Engineering at the Department of Civil Engineering at Abbes Laghrour University of Khenchela (ALGERIA). He has supervised more than 5 PhD and 10 MSc students. Moreover, he has published more than 20 journal papers. His research interests include composite structures, nanocomposites and mechanics of nano-structures, numerical analysis, and programming, especially Maple.

Fouad Bourada holds a PhD degree (2018) in Civil Engineering from Belhadj Bouchaib University of Ain Temouchent, Ain Temouchent (ALGERIA). He is an Associate Professor at the Department of Science and Technology, Center University of Tissemsilt, Ben Hamouda (ALGERIA). His research interests include Plate/beam theories, composite structures, functionally graded structures, nanocomposite structures, nanoplates, nanobeams, and non-local elasticity.

Mohamed Bourada holds a PhD degree (2013) in Civil Engineering from Djillali Liabes University of Sidi Bel Abbes (ALGERIA). He is a Professor at the Department of Civil Engineering, Djillali Liabes University of Sidi Bel Abbes (ALGERIA). His research interests include Topics: Functionally graded material, Plate theory, Beam (structure), Boundary value problems, and Virtual work.

Abdelouahed Tounsi obtained his PhD degree (2002) at the University of Sidi-Bel-Abbes, Bel Abbes (ALGERIA). He is a Professor at the Civil Engineering Department, University of Sidi-Bel-Abbes, Bel Abbes (ALGERIA). He is an active researcher, producing more than 682 papers in index journals. He is also a member of several national and international organizations. His research interests include Plate/beam theories, composite structures, functionally graded structures, nanocomposite structures, nanoplates, nanobeams, and non-local elasticity.

Muzamal Hussain holds a PhD in Mechanics and Energy from the University of Lille (FRANCE). He is an Assistant Professor at National Textile University Faisalabad (Pakistan). Muzamal does research in Discrete Mathematics, Algorithm Analysis, Applied Mathematics, Wave Propagation, Vibration Analysis, and functionally graded structures.